

# Structural behaviour of small GFRP-reinforced seawater sea-sand fiber reinforced concrete culverts

Amirhesam Mashayekhi<sup>a</sup>, Reza Hassanli<sup>a,\*</sup>, Yan Zhuge<sup>a</sup>, Xing Ma<sup>a</sup>, Christopher W.K. Chow<sup>b</sup>, Milad Bazli<sup>c</sup>, Allan Manalo<sup>d</sup>

<sup>a</sup> University of South Australia, UniSA STEM, SA 5095, Australia

<sup>b</sup> Sustainable Infrastructure and Resource Management (SIRM), UniSA STEM, University of South Australia, Mawson Lakes, SA 5095, Australia

<sup>c</sup> Faculty of Science and Technology, Charles Darwin University, Darwin 0810, Australia

<sup>d</sup> Center for Future Materials, School of Engineering, University of Southern Queensland, QLD 4350, Australia

## ARTICLE INFO

### Keywords:

Culverts  
Hybrid fibers  
GFRP  
Shear capacity  
Seawater  
Sea-sand  
Structural performance  
Shear failure  
PVA

## ABSTRACT

This study investigates the structural behaviour of fiber-reinforced seawater sea-sand concrete (FR-SWSSC) culverts employing glass fiber-reinforced polymer (GFRP) bars as internal reinforcements. Eighteen small concrete culverts with a total width of 470 mm and two different total heights of 425 mm and 365 mm, conforming to the Australian standard were subjected to experimental evaluation. The study investigated various parameters, including fiber type (macro polypropylene (PPL), macro twisted polypropylene (TPPL), micro polyvinyl alcohol (PVA), and micro basalt (BA) fibers), fiber hybridization, compression GFRP reinforcement, crown thickness, haunches, and concrete compressive strength. A comprehensive analysis of culvert behaviour was conducted, encompassing load at first crack, crack propagation, load-displacement response at the mid-span of the crown, ultimate load-carrying capacity, energy dissipation, ductility, and failure mode. The results showed that punching shear at the crown was the prevalent failure mode for FR-SWSSC culverts. The ultimate shear capacity, cracking strength, and energy dissipation of culverts were significantly enhanced by the addition of fibers, particularly hybrid fibers (PVA/BA and PPL/PVA). Partial substitution of PPL fiber with PVA resulted in a substantial increase in ultimate strength compared to PPL fiber culvert. The performance and effectiveness of fibers, especially hybrid ones, were significantly influenced by the presence of compression GFRP reinforcement and reduced crown thickness. Haunches had a profound impact on the shear strength of GFRP-reinforced culverts and significantly altered the performance of fibers. This study demonstrates that FR-SWSSC culverts reinforced with GFRP bars and discrete fibres can serve as a sustainable alternative to conventional concrete culverts.

## 1. Introduction

Small concrete culverts (SCC), frequently used under driveways and sidewalks, play a critical role in stormwater management, flood prevention, and transportation network preservation. As shown in Fig. 1, SCCs act as bridges over minor streams and drainage ditches, ensuring water flow. Despite their diverse applications, steel reinforced culverts face durability challenges. Exposed to harsh environments, they endure the detrimental effects of surrounding soil, water containing chemicals and salts, and other substances, leading to long-term damage and corrosion. This significantly reduces their service life and increases maintenance costs. While the prospect of using more sustainable alternatives with non-corrosive reinforcement is appealing, previous studies

have predominantly focused on steel-reinforced large concrete culverts.

Fiber-reinforced polymers (FRPs) offer a compelling alternative to steel in concrete structures due to their superior properties: low weight, high tensile strength, and exceptional corrosion resistance [1–3]. This eliminates corrosion, extending the lifespan of concrete, especially in harsh environments [4]. Among FRPs, glass fiber-reinforced polymer (GFRP) emerges as suitable for reinforcement due to their relative lower cost [1,5]. Studies on GFRP-reinforced culverts demonstrate their adequate load-carrying capacity through acceptable deflection and crack width and impressive long-term performance, maintaining microstructural integrity and mechanical properties over time [6–8]. With exceptional stability against saltwater, chemicals, and alkaline environments, GFRP proves ideal for sustainable concrete alternatives

\* Corresponding author.

E-mail address: [reza.hassanli@unisa.edu.au](mailto:reza.hassanli@unisa.edu.au) (R. Hassanli).

<https://doi.org/10.1016/j.istruc.2024.107492>

Received 20 May 2024; Received in revised form 29 August 2024; Accepted 5 October 2024

Available online 17 October 2024

2352-0124/© 2024 The Author(s). Published by Elsevier Ltd on behalf of Institution of Structural Engineers. This is an open access article under the CC BY license (<http://creativecommons.org/licenses/by/4.0/>).

like seawater and sea-sand concrete (SWSSC) [9–11].

SWSSC made from abundant natural resources, a sustainable alternative with freshwater conservation, reduced transportation and maintenance cost, and exceptional marine environment resilience, proves ideal for coastal and environmental projects like artificial reefs [12]. Its cost-effectiveness makes it particularly attractive in water-scarce regions with limited high-quality aggregate access. While research exists on FRP bars in various SWSSC elements, studies on SWSSC culverts reinforced with FRP bars are scarce. Existing literature demonstrates that GFRP bars exhibit superior durability compared to basalt FRP (BFRP) bars when used in SWSSC [9,11]. Studies on GFRP-reinforced SWSSC slabs and beams also indicate the viability of GFRP bars as a steel alternative with similar shear behaviour [13,14]. The ultimate load of these beams increased with both the reinforcement ratio and the shear span ratio [15]. However, marine exposure can negatively impact bond behaviour, leading to reduced stiffness, ductility, and bond strength [14, 16].

Previous studies employed fibers to improve the mechanical properties of SWSSC. Polyvinyl alcohol (PVA)/basalt (BF) hybridization significantly improved the total energy absorption and residual strength of SWSSC under compression by 44 % and 181 % compared to using mono BF incorporation [17]. While seawater sea-sand recycled aggregate concrete (SSRAC) generally exhibited higher compressive strength than ordinary concrete [18], reinforcing SSRAC with stainless steel fibers (SSF) and polypropylene (PP) fibers improved its mechanical performance. Studies reported that SSF-reinforced SSRAC and PP-reinforced SSRAC resulted in average compressive strengths that were 17.30 % and 2.87 % higher, respectively, compared to plain SSRAC. Additionally, the splitting tensile strengths of these fiber-reinforced SSRACs were 18.48 % and 12.23 % higher, respectively [19]. Furthermore, research has indicated that hybridizing micro-fibers can significantly improve both the flexural strength and fracture energy of SWSSC. Hybrid combinations of PP/BF, or PP/PVA, have been shown to increase fracture energy by 176 % and 290 %, respectively, compared to using PP fibers alone [20].

Multiple studies investigated the use of fibers to enhance the performance of FRP-reinforced SWSSC, particularly addressing bonding strength concerns. Incorporating 0.5 % polyethylene (PE) fibers significantly increased bond strength by 3–10 % [21], while glass fibers improved bond stiffness without significantly impacting FRP bar bond strength [22]. Though FRP bars offer advantages, their lower modulus results in wider cracks and larger deflections compared to steel bars [5, 23]. However, PP and PVA fibers significantly reduced crack width and spacing in SWSSC slabs compared to plain concrete [13]. Additionally, GFRP-RC slabs with plain SWSSC exhibited a 13 % lower cracking moment than ACI 440.1R-15 [24] predictions, but this was mitigated by adding fibers, particularly PP fibers [13]. Furthermore, PP and PVA fibers improved ductility, tensile strength, and energy absorption, and reducing crack formation of SWSSC [25,26]. However, limitations exist for mono-fibers, regardless of size, due to challenges in achieving

uniform distribution and their limited impact on crack control, tensile strength, toughness, and bonding [27,28]. This restricts their applicability and overall potential for enhancing mechanical properties.

Combining micro and macro fibers, chosen strategically for material, volume, aspect ratio, and bond strength, significantly enhances the mechanical performance, ductility, and long-term service life of both normal and SWSSC, overcoming limitations of single-fiber reinforcement [27,28]. Specific fiber combinations like carbon/polypropylene/aramid significantly improved GFRP bar bonding [29], while steel/PVA fibers alongside GFRP bars resulted in substantial increases in bond strength, energy dissipation, and deformation capacity [30]. Hybrid fibers also enhanced shear strength and ultimate load capacity of GFRP-reinforced concrete beams by 55 % to 233 % compared to non-fiber ones [31]. Hybrid steel/polyolefin (PO) fibers effectively improved the shear strength and ductility of GFRP-reinforced beams, shifting failure modes from brittle to ductile [32]. Hybrid fibers outperformed mono fibers in enhancing post-cracking stiffness due to their combined crack resistance properties [33]. Incorporating hybrid basalt/polyolefin fibers and a GFRP laminate into concrete beams with GFRP bars resulted in significant 59 % and 49 % enhancements in maximum yield and ultimate load, respectively, showcasing the effectiveness of hybrid fibers [34].

While previous research has demonstrated the potential application of GFRP bars as an alternative to steel in concrete culverts, limitations have been identified regarding crack width and deformation under load. Aiming to address this gap in knowledge and further enhance both structural performance and sustainability, this research investigates the combined use of non-corrosive GFRP bars and fiber-reinforced seawater and sea-sand concrete (FR-SWSSC). Employing mono- and hybrid-fibers in SWSSC, the study evaluates the mechanical properties, strength, and ductility of GFRP-reinforced culverts at both material and structural levels. Additionally, the research explores the influence of several parameters on performance, including compression reinforcement, slab thickness, haunches, and concrete strength. This study seeks to provide valuable insights into the behaviour of GFRP-reinforced concrete culverts using FR-SWSSC, demonstrating its potential as a viable, cost-effective, and sustainable alternative with enhanced performance.

## 2. Experimental program

### 2.1. Material properties and mixture proportions

SWSSC, designed for a 150 mm slump and 50 MPa compressive strength, adhering to the specifications outlined in AS 1379–2007 [35] and AS 1597.2–2013 [36], respectively, was employed for the culvert construction. Seawater from Adelaide coastal water with significantly elevated chloride and sulfate levels compared to tap water was utilized and carefully stored to prevent contamination. Sea-sand was obtained from Semaphore beach in Adelaide, and meticulously cleaned to remove impurities, served as the fine aggregate. Crushed basalt from a local



Fig. 1. The application of small concrete culverts.

quarry provided the coarse aggregate, with a maximum size of 14 mm. Ordinary Portland cement (OPC) and ground granulated blast furnace slag (GGBS) were employed as cementitious materials. To achieve the desired slump, a polycarboxylate ether-based superplasticizer was added to each mix.





This study investigated the use of mono/hybrid fibers (synthetic and natural) to improve the performance of SWSSC culverts. Untreated micro-fibers (polyvinyl alcohol and basalt) and macro-fibers (polypropylene and twisted polypropylene) were selected for cost-effectiveness. Table 1 details the properties of these fibers provided by the manufacturer. Macro-fibers of similar length but varying aspect ratios and elastic modulus were utilized to evaluate their performance. An environmentally friendly recycled plastic PPL fiber, readily available in the Australian market, commercially named eMesh and manufactured by FIBERCON, was also chosen. Basalt fibers were selected for their high tensile strength, cost-effectiveness, and eco-friendliness. Uniform-length micro-fibers were used to minimize their influence on results.

Two GFRP bar shapes were used to manufacture the culverts: U-shaped and straight, both with a 10 mm diameter and manufactured via pultrusion. Table 2 details the material properties of the GFRP bars, as specified by the manufacturer. The study utilized both mono-fiber and hybrid-fiber to investigate the influence of fibers on SWSSC culverts. Following the approach implemented in previous studies [17,37], four fiber-reinforced mixes were selected: PPL, TPPL, hybrid micro PVA/BA, and hybrid micro/macro PPL/PVA. For comparison, two additional mixes were included: plain SWSSC and high-strength PPL-reinforced SWSSC. Table 3 details the specific mix proportions and Table 4 details their corresponding mechanical properties. The study employed a total fiber volume fraction of 0.66 %, to provide a balance between optimal strength and workability. Increasing the dosage could lead to clumping, while a lower content might not significantly enhance properties as was experience by previous studies [38].

2.2. Test specimens and preparation

A total of 18 GFRP-reinforced concrete culverts were tested which were categorized into five groups as shown Table 5. Group I utilized five SWSSC mixes (Table 3), while Groups II-V investigated the influence of compression reinforcement, crown thickness, haunches, and SWSSC strength, respectively. Fig. 2 presents the details of the culverts, including the size and spacing of the GFRP reinforcement. These

Table 1  
Physical properties of different fibers.

Property	PVA <sup>a</sup>	BA <sup>b</sup>	PPL <sup>c</sup>	TPPL <sup>d</sup>
Specific gravity	1.3	2.8	0.91	0.91
Length (mm)	8	7	47	54
Diameter (μm)	38	15	—	800
Thickness (μm)	—	—	<500	—
Tensile strength (MPa)	1600	2900	400	620
Young's modulus (GPa)	40	85	6	9.5
Chemical resistance	Excellent	Excellent	Excellent	Excellent
Melting point (°C)	225	1450	160	160
Water absorption (% by weight)	<1	<1	Nil	Nil
Alkali resistance	Excellent	—	Excellent	Excellent
Corrosion resistance	Excellent	—	Excellent	Excellent
Shape				

<sup>a</sup> polyvinyl alcohol,  
<sup>b</sup> basalt fiber,  
<sup>c</sup> long polypropylene,  
<sup>d</sup> long twisted polypropylene.

Table 2  
Physical properties of GFRP bars.

Property	Bar type	
	GFRP #3	
Nominal bar diameter (mm)	9.52	
Cross-sectional area (mm <sup>2</sup> )	71	
Tensile elastic modulus (GPa)	60	
Ultimate tensile strength (MPa)	1000	
Strength of Bend (MPa)	Straight Portion	900
	Bend Portion	600
Ultimate tensile strain	0.017	
Glass Transition Temperature, T <sub>g</sub> °	125 °C	

dimensions comply with the Australian code for precast steel reinforced concrete box culverts (AS 1597.1–2010 [39]).

Fig. 3 illustrates the fabrication of culvert specimens. Plywood formworks were built and sealed with silicone for leak prevention (Fig. 3a). GFRP cages were constructed and secured within the formwork using plastic chairs and ties, while lifting lugs were attached for ease of movement (Fig. 3b). Strain gauges were mounted on longitudinal GFRP bars at mid-span for elongation measurement (Fig. 3b). Concrete was vibrated for efficient compaction, especially for FRC culverts. After casting, culverts were covered in plastic for 24 h and demolded after 48 h, following the same curing process as cylindrical and beam specimens. All culverts were maintained under moisture curing conditions for over 45 days prior to testing, ensuring that all specimens reached their maximum strength. For enhanced crack visibility, culverts were painted white and marked with a grid pattern.

2.3. Test setup, instrumentation, and testing procedure

Fig. 4 depicts the culvert test setup, adhering to AS1597.1–2010 guidelines [39]. An 1,800-kN universal testing machine was used to apply load at 0.02 mm/s displacement rate until a 25 % strength reduction was achieved. No lateral load was applied to simulate poor sidefill compaction to simulate the worst-case loading scenario, known to increase crown loads and compromise structural integrity [40,41]. It is important to note that applying lateral load and providing additional support can potentially increase the ultimate strength of culverts [7]. Two steel channels with about 10 mm clearance (Fig. 4) simulated the base slab behaviour and partially restrained leg lateral movements.

**Table 3**  
Mix proportions of SWSSC.

Concrete mix	Total fiber volume fraction (%)	Mix proportions (kg/m <sup>3</sup> )								
		Micro-fiber		Macro-fiber		Binder		Gravel	Seawater	Sea-sand
		PVA	BA	PPL	TPPL	OPC	GGBS			
Plain SWSSC	—	—	—	—	—	144	267	925	222	755
PPL	0.66	—	—	6.0	—	—	—	—	—	—
TPPL	0.66	—	—	—	6.0	—	—	—	—	—
PPL/PVA	0.66	2.86	—	4.0	—	—	—	—	—	—
PVA/BA	0.66	5.72	6.16	—	—	—	—	—	—	—
HS-PPL	0.66	—	—	6.0	—	193	357	925	222	700

**Table 4**  
Mechanical properties of different FR-SWSSC mixes.

Concrete mix	Compressive strength (MPa)	Splitting tensile strength (MPa)	Modulus of rupture (MPa)
Plain SWSSC	47.7	4.34	4.4
PPL	50.5	4.88	4.9
TPPL	56.7	4.95	5.5
PPL/PVA	52.5	5.08	5.1
PVA/BA	55.2	4.80	5.4
HS-PPL	75.5	6.6	6.7

**Table 5**  
Summary of culvert specimens.

Group	Culvert designation	Concrete mix	Slab thickness (mm)	GFRP reinforcement		Span	Height	Objective
				Bottom	Top			
I	C135-G1	Plain SWSSC	135	5 Ø 10	—	320	285	Effect of different fibers
	C135-G1-PL	PPL						
	C135-G1-TP	TPPL						
	C135-G1-PV/PL	PPL/PVA						
	C135-G1-BA/PV	PVA/BA						
II	C135-G2-PL	PPL	135	5 Ø 10	5 Ø 10	320	285	Effect of compression reinforcement
	C135-G2-TP	TPPL						
	C135-G2-PV/PL	PPL/PVA						
III	C80-G1-PL	PPL	80	5 Ø 10	—	320	285	Effect of crown thickness
	C80-G1-TP	TPPL						
	C80-G1-PV/PL	PPL/PVA						
	C80-G1-BA/PV	PVA/BA						
IV	C80-G1-PL-H	PPL	80	5 Ø 10	—	314	285	Effect of haunches
	C80-G1-TP-H	TPPL						
	C80-G1-PV/PL-H	PPL/PVA						
	C80-G1-BA/PV-H	PVA/BA						
V	C135-G1-PL-H	HS-PPL	135	5 Ø 10	—	320	285	Effect of concrete strength
	C135-G2-PL-H	HS-PPL		5 Ø 10	5 Ø 10			

Rubber pad strips between the legs and channels provided cushioning and prevented stress concentration as per AS1597.1–2010 [39]. A 10-mm rubber pad replicating a vehicle wheel and promoting even load distribution was placed on the culvert slab, followed by a rectangular steel bearing block (50 mm × 125 mm surface, 20 mm thickness). A

LVDT positioned beneath the culvert midspan measured its vertical deflection. Two smaller LVDTs attached to the top of the legs (Fig. 4) tracked the expected compression of the rubber pads placed under the culvert legs. Two strain gauges, capable of measuring large strains, were attached to the middle of GFRP bars (top and bottom) in the crown to

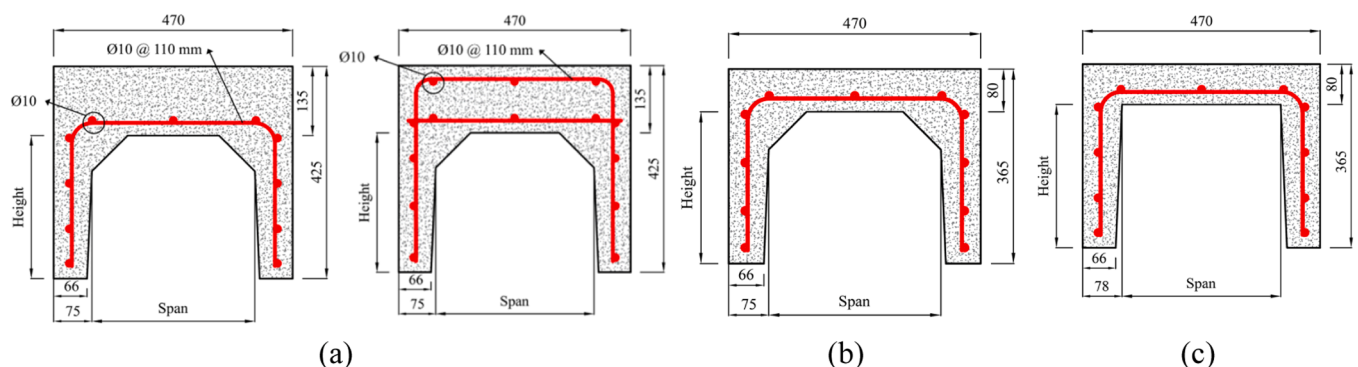


**Fig. 2.** The details of culverts, a) group I, II, and V, b) group III, and c) group IV.



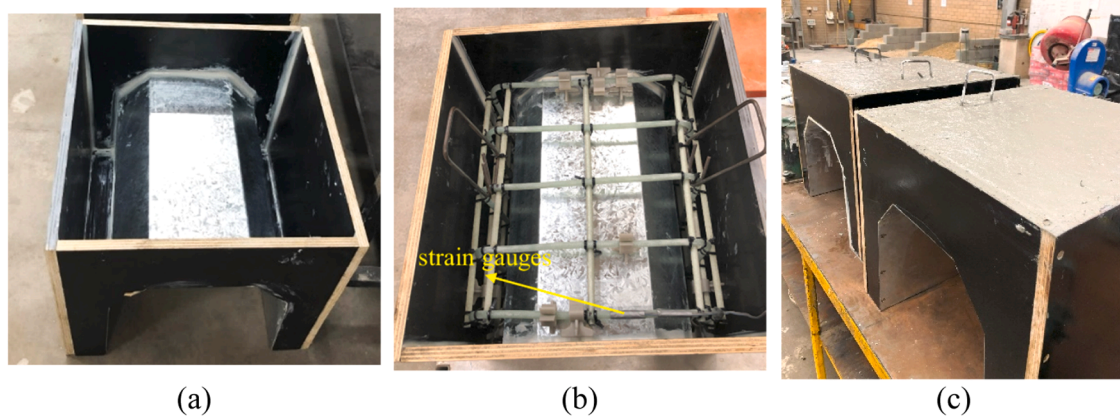


**Fig. 3.** The fabrication of culvert specimens, (a) plywood formwork sealed with silicone, (b) GFRP cage secured in formwork using plastic chairs and ties, and (c) casted SWSSC culverts.

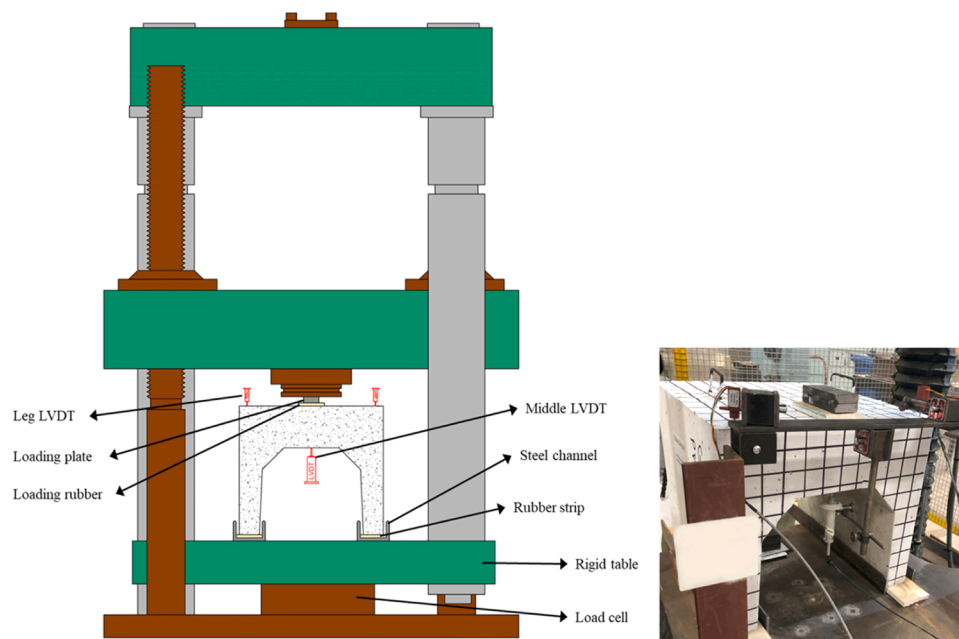


**Fig. 4.** Test setup.

monitor their strain behaviour. To protect them during concrete casting, the gauges were covered with duct tape and their wires carefully positioned.

### 3. Test results and observations

This section presents the results of two distinct parts of this study: (1) material testing of SWSSC, and (2) evaluation of the impact of different fibers on the performance of GFRP-reinforced SWSSC culverts.

#### 3.1. Behaviour of SWSSC

The results of material testing performed on fiber-reinforced SWSSC are presented in detail in the [Supplementary Information](#).

#### 3.2. Behaviour of GFRP-reinforced SWSSC culverts

Five groups of GFRP-reinforced culverts were studied to assess the influence of various parameters on their performance. Group I examined the effect of fiber type (mono and hybrid), Group II investigated the

impact of compression reinforcement, Group III focused on the influence of crown thickness, Group IV evaluated the role of haunches, and Group V studied the effect of concrete strength. The key observations from the testing of these culverts will be presented in the following sections.

##### 3.2.1. Crack pattern and failure mode

**Fig. 5** shows the crack pattern observed in the culverts at the failure point. The presence of a primary shear crack diagonally through the haunch, aligns with observations in the previous studies on GFRP culverts [7]. Unlike steel-reinforced culverts, where flexural cracks are predominant [42], GFRP-reinforced culverts are more prone to shear cracks. This is primarily attributed to the lower modulus of elasticity of GFRP reinforcement, which significantly influences crack width limitations [7]. Moreover, the dowel action of longitudinal reinforcement is negligible in GFRP bars due to their limited shear capacity in the transverse direction [7]. Notably, all specimens initially exhibited flexural cracks before transitioning to shear-dominant failure. This can be attributed to the high tensile stress at the bottom of the crown, which caused flexural cracks to form initially, as observed in previous studies on one-way and two-way GFRP-reinforced slabs [13,43–45].

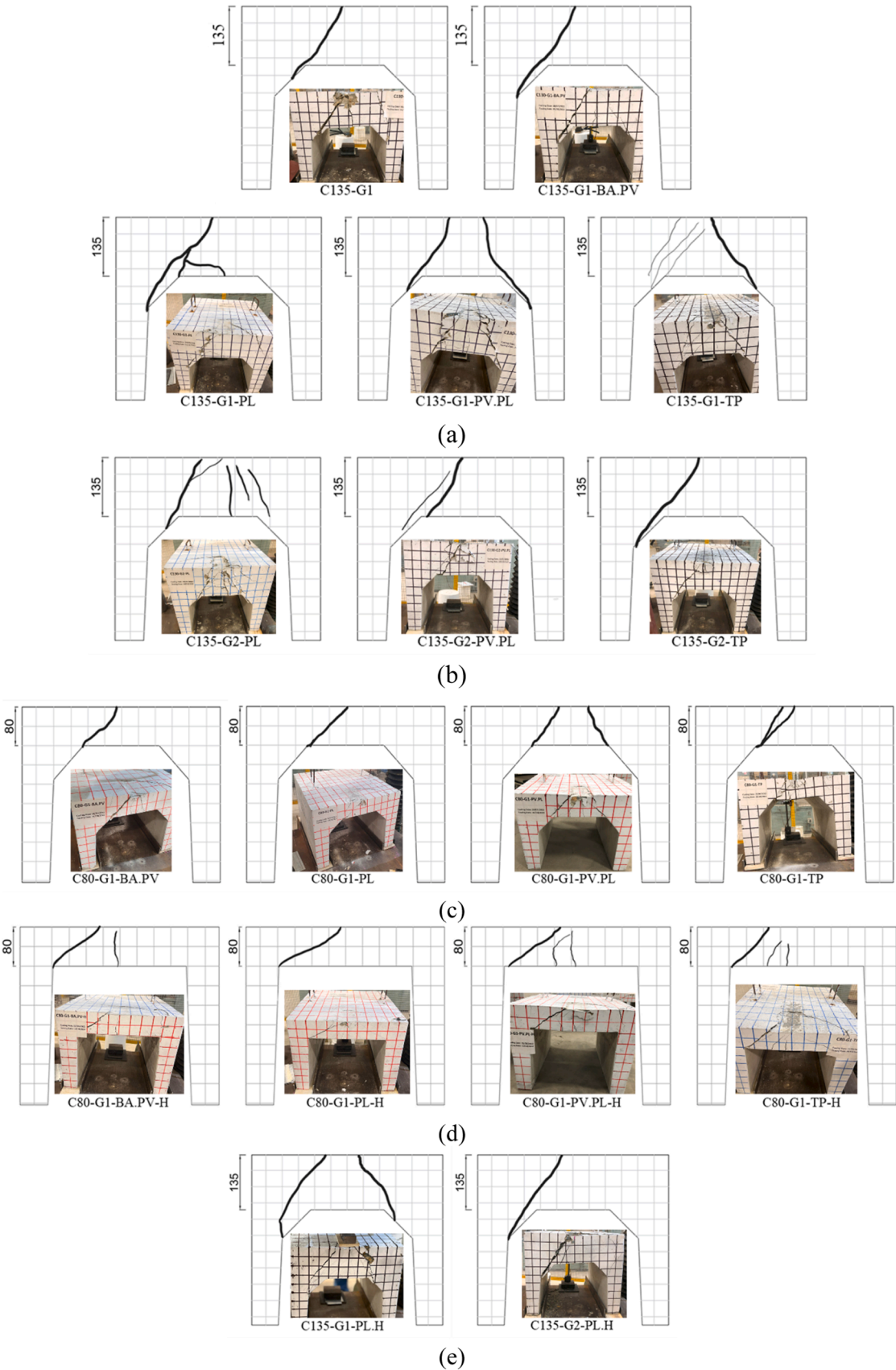


Fig. 5. Failure mode of the fiber-reinforced SWSSC culverts, a) group I, b) group II, c) group III, d) group IV, and e) group V.

Fibers in Group I extended the length of the primary shear crack, initiating it from the load point and extending towards the end or middle of the haunch. Fiber-reinforced specimens typically failed with one dominant shear crack, except for the hybrid PPL/PVA fiber-reinforced concrete. This hybrid specimen developed two cracks, highlighting its ability to significantly increase shear strength. Additionally, this behaviour was also observed in Group III specimens with an 80 mm crown. This enhancement can be attributed to the synergistic effect of PPL/PVA hybridization, which resulted in a more uniform distribution of shear stresses. This, in turn, led to the formation of two primary shear cracks and a subsequent increase in the ultimate strength of culvert.

Reducing the crown thickness (group III) altered the shear failure path, increasing its angle and causing early failure before engaging the haunches, negating their influence on shear strength. Removing the haunches (group IV) further modified the path, directing it towards the leg tips with a single, dominant crack observed consistently. These

findings suggest that haunches can significantly enhance the shear strength of concrete culverts, provided that the crown thickness is adequate. By reducing the effective span length, haunches lead to a lower span-to-depth ratio. This reduction in span-to-depth ratio is known to increase the ultimate shear strength of concrete culverts, similar to the behaviour of concrete beams [46]. PPL fibers effectively limited initial cracking in group IV, while replacing a portion of PPL with PVA fibers (hybrid PPL/PVA) resulted in more pronounced flexural cracks at mid-span. This suggested that the addition of PVA fibers resulted in a more uniform distribution of stress in the tensile portion of the section. TPPL fibers, due to their distribution, displayed a unique shear crack path with a higher angle and greater distance from the loading point. The uniform distribution of TPPL fibers and their strong bond with the concrete matrix effectively transferred shear stresses, preventing crack propagation, and resulting in a distinct shear crack path and angle.

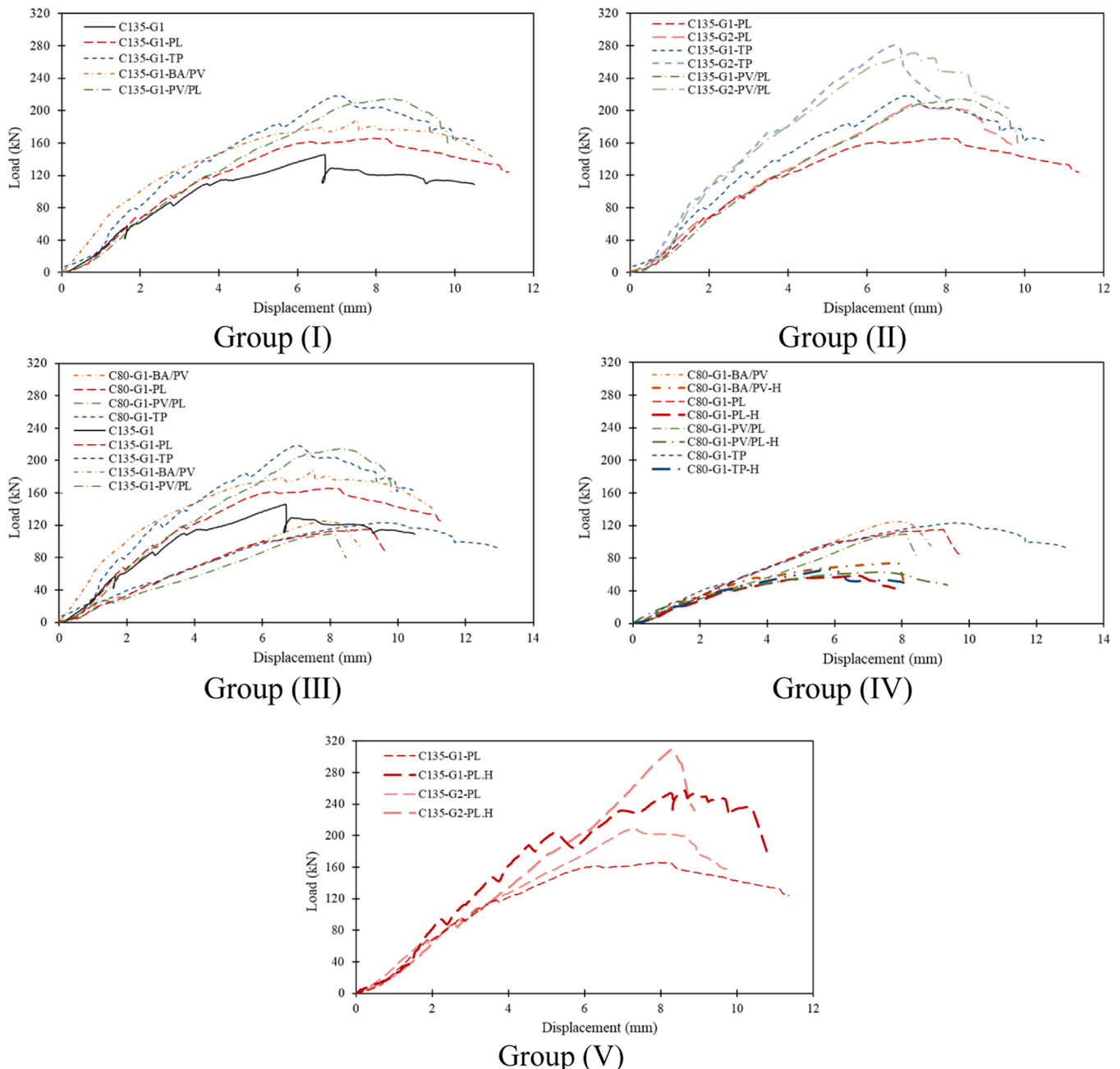


Fig. 6. The load versus mid-span deflection curves for all culvert groups.

Adding compression reinforcement (group II) considerably altered the shear crack behaviour of hybrid PPL/PVA fiber specimens, resulting in a single primary shear crack. In addition, PPL and TPPL fibers displayed contrasting crack patterns and angles. While G135-G2-PL specimens exhibited a higher number of high-angle cracks compared to G135-G2-TP specimens, the crack lengths were shorter. These findings may be attributed to the presence of compression reinforcement, which can redistribute stresses within the section and potentially reduce the concentration of shear stresses at critical locations. This could potentially alter the failure mode of culverts reinforced with different fiber types. When concrete strength was increased (group V), G135-G1-PL.H developed more primary shear cracks. In contrast, G135-G2-PL.H displayed fewer cracks but fully utilized the haunch capacity. The primary crack shifted towards the haunch end and grew longer compared to G135-G2-PL.

### 3.2.2. Load–deflection behaviour

Fig. 6 displays the load versus mid-span deflection curves for all culvert groups, revealing three distinct phases. The initial phase was linear and identical for all groups, followed by a second linear phase with a smaller slope, signifying reduced stiffness due to concrete cracking and lower effective inertia moment [14]. This slope was influenced by factors like fiber distribution, modulus, and length [31]. The final phase exhibited varying slopes in post-peak behaviour, influenced by the type and distribution of fibers.

Specimen C135-G1 with no fiber exhibited a significant (20 %) decrease in load following initial cracking, attributed to the low GFRP bar elastic modulus replicating previous observations [32,33,47]. This drop persisted after the peak load. Inclusion of fibers, both mono and hybrid, mitigated this drop and facilitated a smooth transition from each stage. Fibers achieved this by arresting major cracks, redistributing stresses, and enhancing the overall performance of culvert [33]. Both fiber properties and quantity significantly influence this transition behaviour [31,33]. Prior research indicated that hybrid fibers were more effective than mono fibers in improving cracking strength [48], this finding confirmed in this study for GFRP-reinforced concrete culverts.

The addition of compression reinforcement significantly enhanced the culvert's stiffness, both before and after the peak load. This can be attributed to the improved axial stiffness provided by the compression reinforcement, which can substantially increase the overall stiffness. Replacing some PPL fibers with PVA fibers led to a notable increase in stiffness compared to using PPL fibers alone. This was likely due to the higher tensile strength of PVA fibers and their stronger bond with the concrete matrix, creating a positive synergy with PPL fibers that contributed to increased stiffness under tensile stresses. Comparing PPL and TPPL fibers, the top reinforcement effect on stiffness was more pronounced with TPPL fibers. Reducing the crown thickness by 40 % considerably decreased pre-peak stiffness. This could be attributed to the smaller cross-sectional area, which results in a decrease in the bending moment capacity of culvert. Consequently, the overall stiffness was reduced. While specimens using different fibers exhibited a smooth transition to the post-peak phase, reduced thickness resulted in a sudden load drop after peak, except for specimens with TPPL fibers. This could be attributed to the improved distribution and flexibility of TPPL fibers, leading to a higher concentration of fibers in the failure plane and better post-peak behaviour.

The removal of haunches significantly impacted the pre-peak stiffness of C80 specimens, resulting in a decrease. This reduction could be attributed to the decreased section modulus, which ultimately leads to reduced stiffness. Partially replacing PPL fibers with PVA fibers improved the post-peak behaviour, offering better ductility. This enhancement could be attributed to the improved bonding strength between PPL fibers and the concrete matrix resulting from the addition of PVA fibers. This stronger bond contributed to enhanced crack bridging and improved ductility. TPPL fiber-reinforced culverts were

more sensitive to haunch removal, experiencing a sudden drop in load-carrying capacity after reaching their peak. Deflection at peak point also decreased except for culverts reinforced with hybrid PPL/PVA fibers. Higher concrete strength increased pre-peak stiffness in both one and two-layer PPL fiber-reinforced culverts, but also resulted in a more abrupt post-peak drop. Specimens with only bottom reinforcement displayed drops during both pre-peak and post-peak phases, while those with top reinforcement exhibited less significant drops. This could be attributed to the higher bonding strength of PPL fibers with SWSSC at higher strengths, leading to prevent their pulling out during loading.

### 3.2.3. GFRP Strain

Fig. 7 shows that all tested GFRP specimens experienced strains lower than their ultimate tensile capacity (17000  $\mu\epsilon$ ), indicating non-rupture at failure. Group I specimens exhibited failure strains ranging from 47.2 % to 73.8 % of ultimate (8028 to 12556  $\mu\epsilon$ ). Initially, strains were low but significantly increased after flexural crack initiation as GFRP bars took on tensile stress. During this stage, fibers in the tension section effectively contributed to tensile stress reduction, lowering GFRP strain values [32]. Hybrid PPL/PVA decreased maximum bottom reinforcement strain by 20 % compared to mono PPL fiber, despite increasing ultimate strength, suggesting a suitable reinforcing system of hybrid PPL/PVA that improves both shear and flexural strength. PPL and TPPL resulted in similar maximum GFRP strain, but TPPL offered higher shear strength. This enhancement could be attributed to the improved distribution and bonding strength of TPPL fibers, which led to a more uniform distribution of shear stresses. C135-G1-BA/PV had the lowest GFRP strain among all fibers, indicating that PVA/BA improved shear strength, allowing the culvert to carry more flexural strength by C135-G1-BA/PV.

Adding top reinforcement significantly reduced the maximum bottom GFRP bar strain in C135-G2-PL specimens by 33 %. This decrease stemmed from increased crown stiffness and reduced mid-span deflection, which led to lower tensile strain in the bottom GFRP reinforcement. The effect was consistent in both C135-G2-PL and C135-G2-PV/PL specimens. However, the tensile strain in the C135-G2-TP specimen remained like that of C135-G1-TP. This discrepancy between PPL and TPPL specimens likely arises due to the superior distribution and flexibility of TPPL fibers.

Removing haunches on C80 culverts had a contrasting effect on strain, increasing it for C80-G1-BA/PV-H while reducing it for others. Despite the expected increase in deflection due to the increased span length, shear failure occurred first and limited deflection, except for C80-G1-BA/PV-H where tensile strain increased instead. Similarly, increasing concrete strength led to a slight strain increase against the anticipated decrease. This was attributed to the improved shear strength, which resulted in higher tensile stress in the bottom GFRP bars.

## 4. Discussion

### 4.1. Group I: effect of mono and hybrid fibers

Fig. 8 shows the typical stress and strain distribution of the crown section of culverts using ACI 440.1R-15 [49]. The depth of neutral axis along with tensile and compression forces are also provided in Table 6. In this study the contribution of fibers in tension part was considered based on definition of ACI 544.4 R-88 [50] in Eq. (1), previously used for both steel and synthetic fibers [51]. Based on the design of the culverts according to ACI 440.1R-15 and AASHTO LRFD [52], all culverts of group I had  $\rho_f > \rho_{fb}$ , indicating over reinforced section.

$$\sigma_{t,FRC} = 0.00772 \frac{l_{fiber}}{d_{fiber}} \rho_{fiber} F_{be} \quad (MPa) \quad (1)$$

where  $l_{fiber}$  is fiber length,  $d_{fiber}$  is fiber diameter,  $\rho_{fiber}$  is percent by volume of fibers and  $F_{be}$  is bond efficiency of the fiber which varies from



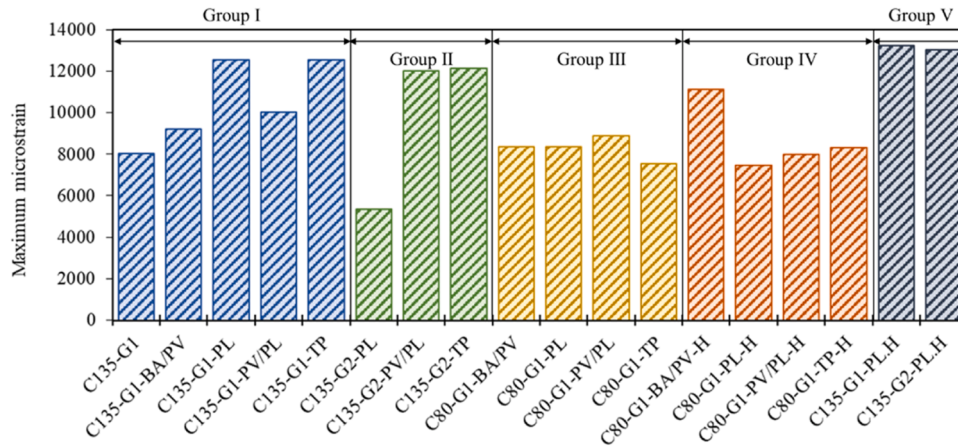


Fig. 7. The maximum strain of GFRP bars for all culvert groups.

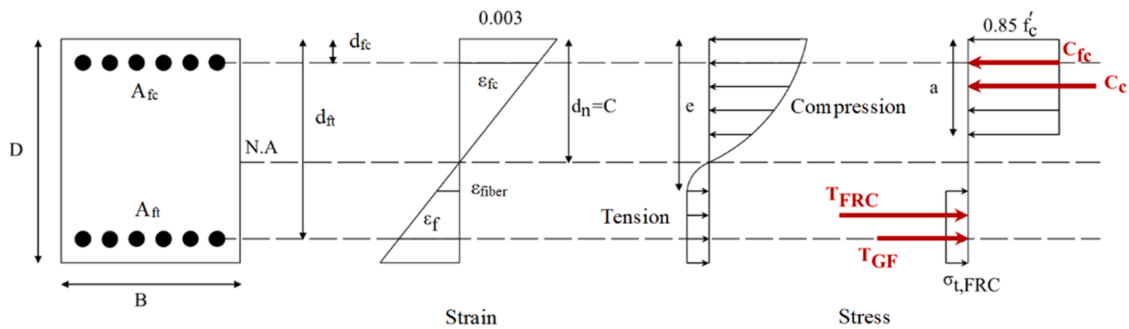


Fig. 8. Typical distribution of stress and strain within the crown cross-section of GFRP fiber-reinforced culverts.

Table 6

Values of key parameters in Fig. 8.

Group	Culvert designation	$d_n$ (mm)	$e$ (mm)	$C_c$ (kN)	$T_{FRC}$ (kN)	$T_{GF}$ (kN)	$\sigma_{t,FRC}$ (MPa)
I	C135-G1	18.8	18.8	324.0	—	324.0	—
	C135-G1-PL	22.0	22.2	432.0	84.2	347.9	1.49
	C135-G1-TP	20.4	20.9	351.7	27.3	324.4	0.48
	C135-G1-PV/PL	19.7	20.1	386.0	38.5	347.5	0.67
	C135-G1-BA/PV	18.2	18.4	381.0	20.1	360.9	0.34
II	C135-G2-PL	21.9	22.5	377.6	27.0	324.4	0.48
	C135-G2-TP	21.2	21.6	414.9	38.0	347.5	0.67
	C135-G2-PV/PL	19.9	20.1	416.8	19.8	360.9	0.34
III	C80-G1-PL	13.8	13.9	287.4	49.3	238.1	1.49
	C80-G1-TP	12.5	12.8	248.8	16.1	232.7	0.48
	C80-G1-PV/PL	13.0	13.3	249.3	22.3	226.9	0.67
	C80-G1-BA/PV	11.8	12.0	253.8	11.7	242.1	0.34
IV	C80-G1-PL-H	14.3	14.5	277.5	48.9	228.6	1.49
	C80-G1-TP-H	13.2	13.6	231.6	15.9	215.7	0.48
	C80-G1-PV/PL-H	13.4	13.6	242.8	22.2	220.5	0.67
	C80-G1-BA/PV-H	12.5	12.6	238.3	11.6	226.7	0.34
V	C135-G1-PL-H	16.3	16.7	444.3	28.3	416.0	0.48
	C135-G2-PL-H	18.0	18.5	490.9	27.9	416.0	0.48

1.0 to 1.2 depending upon fiber characteristics.

#### 4.1.1. Ultimate strength

Fig. 9 demonstrates the significant effect of fiber addition on culvert strength. PPL fibers alone increased ultimate strength by 13.6 %, while TPPL fibers offered a substantial 49.7 % improvement. This aligns with prior research [53] on the positive impact of macro PP fiber on shear strength of concrete culverts. TPPL exhibited a 31.8 % higher ultimate strength over PPL fiber. This enhancement can be attributed to the superior distribution, flexibility, and bonding strength of TPPL, as

observed in the scanning electron microscopy (SEM) analysis presented in Fig. S5, Supplementary Information. Additionally, the higher compressive strength achieved by TPPL-reinforced concrete at 45 days translated to increased shear and ultimate strength compared to PPL-reinforced concrete. Hybrid PPL/PVA fibers resulted in a 47.1 % increase in ultimate strength compared to plain culverts and a 29.5 % increase compared to PPL-reinforced culverts. This improvement could be attributed to the potential synergistic effect of PVA fibers enhancing the bonding strength of PPL fibers, as was observed in the tensile and compressive strength tests of FR-SWSSC mixtures. Fig. 10 presents SEM

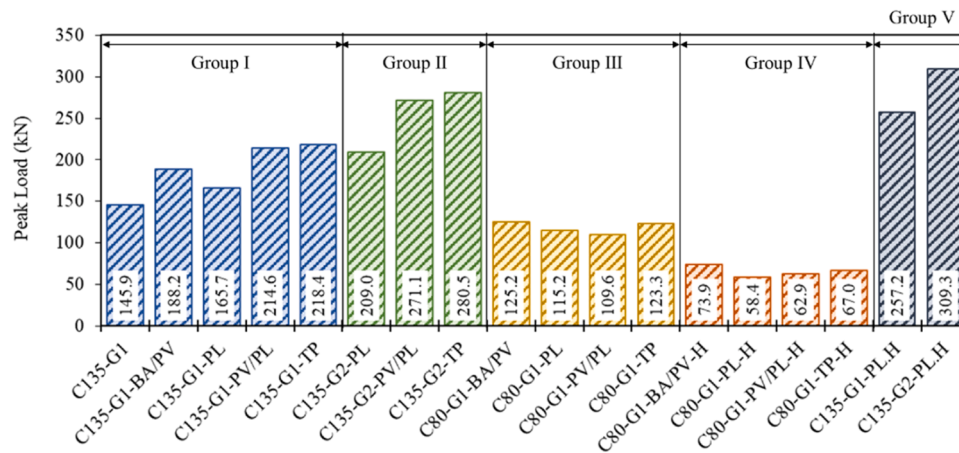


Fig. 9. The ultimate strength of culverts for all groups.

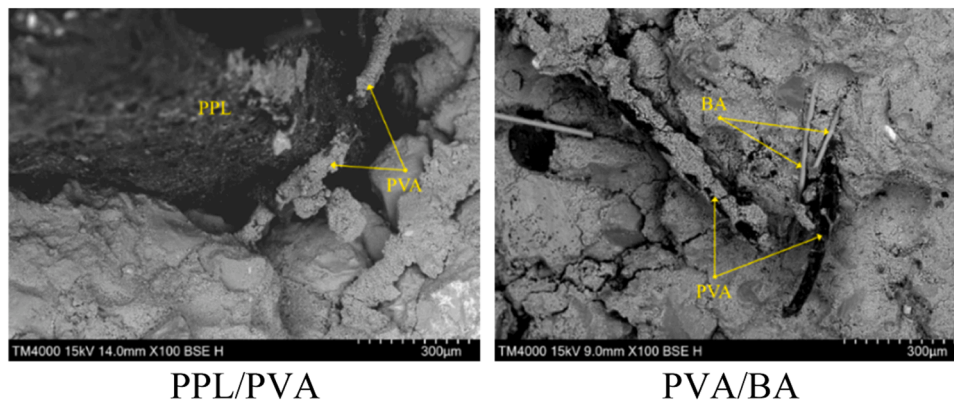


Fig. 10. Synergistic hybridization of PPL/PVA and PVA/BA in SWSSC.

images of hybrid PPL/PVA and hybrid PVA/BA, revealing that the chemical bonding of PVA fibers significantly improved the bond between PPL and BA with SWSSC, consistent with observations from previous studies [17]. As illustrated in Fig. 10, the complementary action of PVA and PPL fibers in the hybrid system likely led to improved PPL fiber-matrix adhesion, resulting in enhanced tensile and compressive strength, ultimately contributing to increased shear strength of the concrete. The hydroxyl groups of PVA fiber contributed to chemical bonding and improved the inter-locking strength of concrete

components [13,44]. Micro-fiber hybridization (PVA/BA) achieved a 29 % strength increase compared to plain culverts and a 13.6 % increase over PPL fibers, highlighting the contribution of the superior strength and stiffness of BA fiber to culvert performance. Material testing revealed a significant increase in compressive strength for SWSSC containing a hybrid PVA/BA fiber compared to PPL fibers alone. This enhancement can be attributed to the synergistic behaviour of BA and PVA fibers, as observed in Fig. 10. BA fibers likely improved the interfacial bonding strength of PVA fibers, aligning with findings from

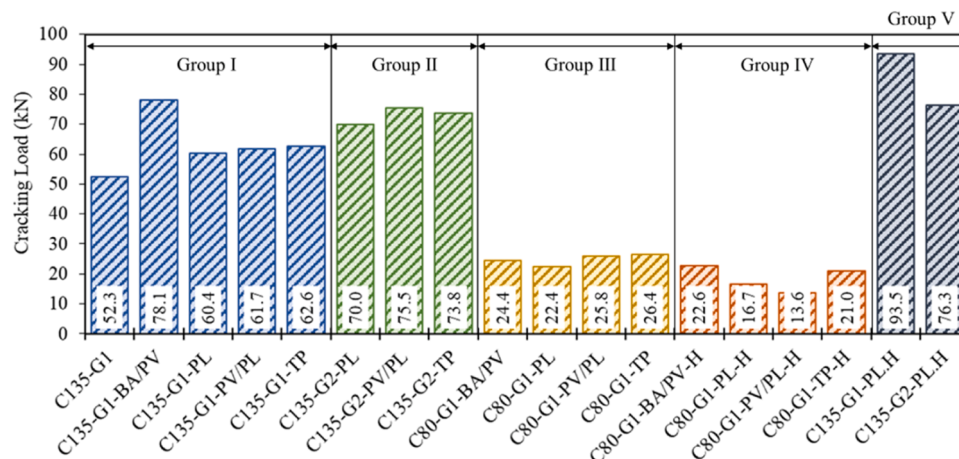


Fig. 11. The cracking strength ( $P_{cr}$ ) of culverts for all groups.

previous study [17]. This improved compressive strength, in turn, resulted in higher shear strength, which played a crucial role in achieving the observed increase in ultimate strength of the SWSSC culverts.

#### 4.1.2. Cracking strength ( $P_{cr}$ )

As shown in Fig. 11, fiber inclusion significantly improved the cracking strength and serviceability of culverts, aligning with previous research on GFRP-reinforced beams [33]. PVA/BA hybridization led to the highest increase (49.3 %) compared to plain concrete, attributed to its strong ability to bridge micro-cracks. While PPL fibers exhibited superior tensile and flexural strength in material testing, PVA/BF achieved a 29.3 % greater cracking strength. TPPL and PPL fibers increased cracking strength by 19.7 % and 15.5 %, respectively, with PPL/PVA hybridization demonstrating an 18 % increase, exceeding mono PPL fibers. Similar results were observed in steel-reinforced beams, where hybrid fibers improved serviceability by reducing deflections and crack widths [47]. PVA/BF incorporation further increased cracking strength by facilitating tensile stress transfer from GFRP reinforcement. Overall, fiber addition delays cracking and increases concrete tensile strength, as evidenced by the material testing results presented in Fig. S4 (Supplementary Information), directly impacting the first crack appearance in culverts [31].

#### 4.1.3. Energy dissipation ( $E_{tot}$ )

Energy dissipation capacity ( $E_{tot}$ ), also known as toughness, is calculated as the area under the load-deflection curve up to the ultimate displacement [47]. The ultimate capacity is typically defined as the point where the load drops by more than 10–30 % of the peak load of the tested specimen [32]. In this study, 25 % drop from the peak load was considered the ultimate capacity. Eq. (2) below was used to compute the energy absorption capacity, with results presented in Fig. 12.

$$E_{tot} = \int_0^P P d\delta \quad (2)$$

Adding fibers significantly increased the total energy dissipation of the specimens, with hybrid PVA/BA and TPPL fibers being the most effective, leading to increases of 49 % and 47 % respectively compared to the control specimen. TPPL fibers absorbed 13 % more energy than PPL fibers, while partially replacing PPL with PVA maintained similar total energy absorption but shifted the distribution, increasing pre-peak energy by 18 % and decreasing post-peak energy. Notably, hybrid PPL/PVA displayed the highest pre-peak energy dissipation, exceeding the control specimen by 73 %, potentially due to the combined effect of the micro-crack bridging of PVA and its synergy with PPL in enhancing bonding strength. This aligns with previous research [47]. Hybridization

of micro-fibers (PVA/BA) also led to significant energy absorption across both stages, surpassing PPL fibers by 21 % and 11 % in post-peak and pre-peak, respectively. This, along with its 14.6 % higher total energy absorption compared to PPL, can be attributed to the improved shear capacity of PVA/BA and micro-crack bridging capabilities. Furthermore, the higher compressive strength and modulus of rupture exhibited by the hybrid PVA/BA fibers compared to PPL fibers contributed positively to achieving greater energy absorption capacity.

#### 4.1.4. Ductility ( $\mu_e$ )

Ductility, the ability to deform plastically before failure, cannot be measured using yielding for FRP-reinforced concrete members. In such cases, energy-based ductility serves as a toughness measure [33,54]. This study uses an energy approach to measure ductility in GFRP-reinforced small culverts. Ductility factor ( $\mu_e$ ), an indirect measure for FRP-reinforced members, is defined as the ratio of total energy to elastic energy (Eq. 3).

$$\mu_e = \frac{1}{2} \left( \frac{E_{tot}}{E_{el}} + 1 \right) \quad (3)$$

$E_{el}$  represents elastic energy dissipated and is calculated as the area of the triangle formed at ultimate load by a line matching the initial linear portion of the load-deflection curve [54].  $E_{tot}$  denotes total energy under the load-deflection curve [47].

Fig. 13 presents the ductility of culverts across different groups, highlighting the significant impact of fiber type, distribution, and bonding strength on ductility. While prior research on GFRP-reinforced beams suggested positive effects of fibers on ductility [33], this study reveals diverse responses in SWSSC culverts. Group I specimens showed the highest ductility (3.95) with hybrid PVA/BA fibers, exceeding plain concrete by 34 %. This improvement stems from the even distribution of fibers, bridging micro-cracks and promoting inelastic energy absorption. PPL and TPPL fibers resulted in ductility values of 3.25 and 2.63, respectively. TPPL slightly increased elastic behaviour due to its improved distribution and bonding strength, leading to increased stiffness in the initial phase. Conversely, the lower bond strength of PPL favoured pull-out and enhanced inelastic behaviour. Partial replacement of PPL with PVA significantly reduced ductility by 36 %. PVA improved the bonding strength of PPL and micro-crack bridging ability, enhancing elastic behaviour after the first crack (higher deflection at peak-point) than PPL. However, it led to lower ultimate deflection, indicating better inelastic behaviour in PPL-reinforced culverts.

#### 4.2. Group II: effect of compression reinforcement

ACI 440.1R-15 [49] recommends neglecting the compressive

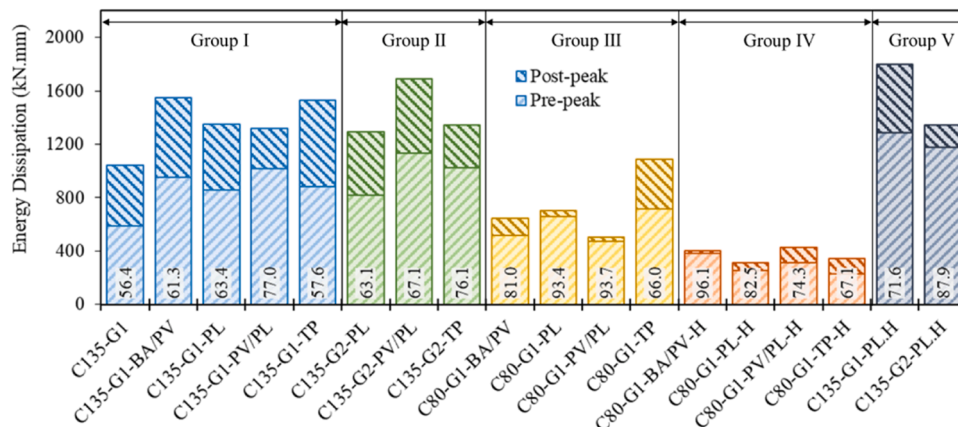


Fig. 12. The energy dissipation ( $E_{tot}$ ) of culverts for all groups (the values in each column represent the percentage of pre-peak energy dissipation to the total energy dissipation).



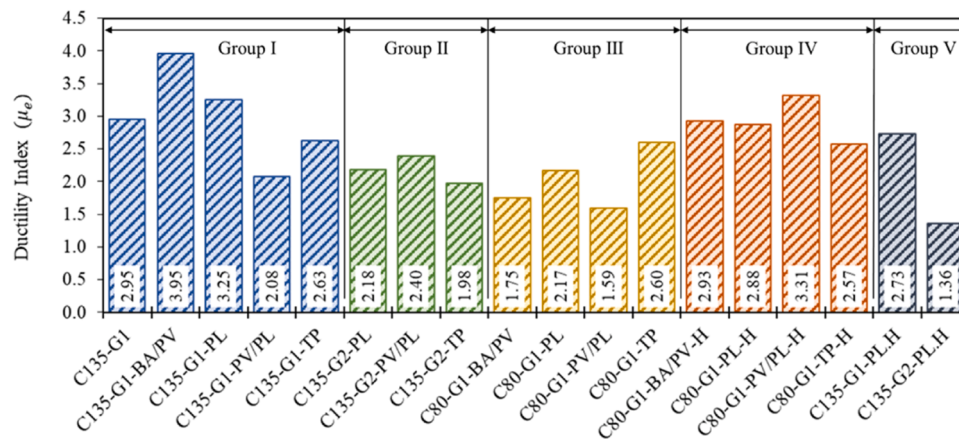


Fig. 13. The ductility index ( $\mu_e$ ) of culverts for all groups.

strength of FRP bars due to its significant deviation from tensile strength. As shown in Fig. 8 and Table 6, adding top reinforcement increased the neutral axis depth ( $d_n$ ), resulting in a reduced tension section and consequently, a decrease in the tensile force ( $T_{FRC}$ ) across all fibers. Additionally, the compression force of concrete ( $C_c$ ) increased due to the enlarged compression section.

Adding top reinforcement to culverts substantially improved their shear performance, with a 26.1 %–28.4 % increase in ultimate strength and a 15.9 %–22.4 % increase in first-cracking strength. While minimally impacting the influence of fibers on ultimate strength, it slightly increased first-cracking strength for hybrid PPL/PVA and TPPL fibers. However, top reinforcement addition resulted in a 4.3 % to 12.3 % decline in total energy dissipation and a 24.7 % to 33 % reduction in ductility for PPL and TPPL reinforced specimens, except for hybrid PVA/PPL fibers which resulted in a 28.1 % and 15.3 % increase, respectively. This was attributed to improved elastic energy and lower deflection at peak-point, leading to decreased inelastic energy and ultimately lower ductility. Additionally, PPL fibers, due to their inferior distribution and bonding, led to a more substantial reduction in inelastic energy and ultimate strength compared to TPPL fibers. While TPPL fibers absorbed more total energy than PPL fibers, adding top reinforcement reduced it more for TPPL fibers due to its better distribution and flexibility being more impacted by the reduced tension section.

Adding top reinforcement improved the ultimate strength of both PPL/PVA and PPL fiber-reinforced specimens by around 26 %, attributed to the enhanced compression force and improved shear strength. However, its impact on ductility and energy absorption differed. While PPL/PVA experienced a 15 % increase in ductility and a 28 % increase in energy absorption, PPL fiber exhibited a 33 % decrease in ductility and a 4.3 % decrease in energy absorption. Notably, top reinforcement significantly increased the stiffness of the culvert with hybrid PPL/PVA fibers by about 51 %, highlighting the significant role of PVA fibers in enhancing stiffness and shear strength in small culverts. Furthermore, PVA fibers boosted both elastic and inelastic energy absorption, contributing to the improved ductility of hybrid PPL/PVA. Conversely, PPL fibers alone resulted in increased elastic energy without affecting stiffness, leading to decreased inelastic energy and ductility.

#### 4.3. Group III: effect of crown thickness

Reducing the crown thickness ( $t_{top}$ ) by 40 % significantly reduced the cracking strength of fiber-reinforced SWSSC culverts, as evidenced by lower  $T_{GF}$ ,  $T_{FRC}$ , and  $C_c$  values (Fig. 8, Table 6). Both fiber type and crown thickness significantly influenced cracking, shear behaviour, energy absorption, and ductility. PVA/BA and PPL fibers caused the largest reductions in cracking strength (68.8 % and 62.9 %, respectively), while TPPL and hybrid PPL/PVA were less sensitive (57.8 % and

58.2 % reduction). Reducing the crown thickness also significantly decreased both the ultimate strength and the energy absorption capacity. The reduction in ultimate strength ranged from 30.5 % to 48.9 %, while the reduction in energy absorption ranged from 29.1 % to 61.6 %. These findings align with previous studies on GFRP-reinforced beams, which demonstrated that increasing the beam depth has a noticeable effect on energy absorption, ultimate shear capacity, and initial flexural cracking [14,47].

Comparing PPL and TPPL fibers, reducing slab thickness revealed interesting effects. While the gap in ultimate strength narrowed from 31.8 % to 7 %, the difference in cracking strength rose from 3.6 % to 17.9 %. This indicates that TPPL fibers, though less impactful on ultimate strength, significantly improve cracking strength when used in thinner slabs. Furthermore, TPPL exhibited superior total energy absorption (55 % increase), a 7-fold increase in post-peak energy absorption, and a 19.7 % higher  $\mu_e$  compared to PPL. However, C135-G1-PL showed a higher  $\mu_e$  than C135-G1-TP. This can be attributed to the superior distribution, flexibility, and bonding strength of TPPL fibers, leading to improved stress distribution and crack bridging in thinner slabs. Notably, reducing slab thickness significantly enhanced the post-peak behaviour and inelastic energy of TPPL-reinforced culverts, but considerably reduced their shear strength.

Replacing part of PPL with PVA in C80-G1-PV/PL significantly impacted its strength and energy absorption. While cracking strength increased by 15 % compared to C80-G1-PL, ultimate strength decreased by 4.9 %. However, thicker crowns reversed this trend, with C135-G1-PV/PL exhibiting a 30 % higher ultimate strength than C135-G1-PL. This suggests that PPL/PVA hybridization enhances cracking resistance but can compromise shear strength when used with thinner slabs. Hybridization led to a 27.9 % decrease in  $E_{tot}$  and a 26.7 % decrease in  $\mu_e$  compared to C80-G1-PL, indicating increased elastic energy, and

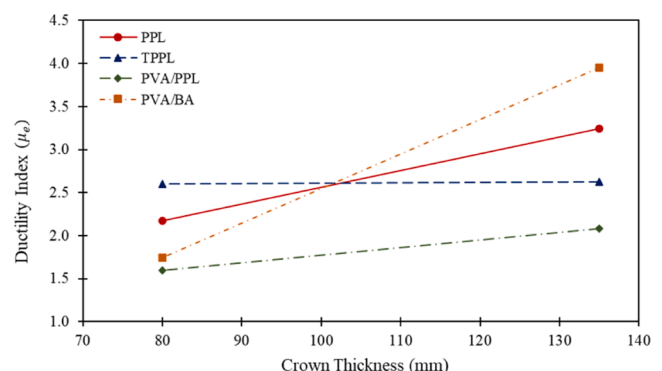


Fig. 14. Influence of crown thickness on ductility index ( $\mu_e$ ) for various fibers.



decreased inelastic energy due to partial replacement of PPL fibers. This suggests that for thinner crowns, the proportion of PPL fibers significantly influenced the ultimate shear strength, ductility, and energy absorption. However, for thicker crowns, PVA fibers demonstrated effectiveness in improving the bonding strength of PPL fibers and providing a positive synergistic effect.

Hybridization with PVA/BA improved the cracking strength of concrete slabs by 8.9 % compared to using PPL alone, with the effect increasing for thicker slabs (135 mm). Reducing the crown thickness by 40 % significantly reduced the total, pre-peak, and post-peak energy absorption of PVA/BA by 59 %, 45 %, and 80 %, respectively, highlighting its strong dependence on slab thickness. Notably, decreasing thickness also considerably lowered ductility for both PVA/BA and PPL, with reductions of 56 % and 33 % in  $\mu_e$ , respectively. In conclusion, a strong correlation between ductility and crown thickness was observed for culverts reinforced with either hybrid PVA/BA or mono PPL fibers, as shown in Fig. 14. This could be attributed to a more even distribution of stresses within the thicker crown section, which reduced stress concentrations. This allowed the fibers to be more effective in bridging and preventing cracks, resulting in higher ductility. When a thinner crown thickness was used, the increased stress concentration limited the effectiveness of the fibers. Accordingly, PVA/BA hybridization, due to the lack of long fibers, experienced a significant reduction in energy absorption and ductility. TPPL fibers exhibited better post-peak behaviour due to their better distribution compared to PPL fibers, which resulted in higher ductility for a lower crown thickness.

#### 4.4. Group IV: effect of haunches

Removing the haunches in the culverts increased the effective span of the crown, significantly reducing shear strength, as observed in GFRP-reinforced beams with increased shear-span ratios [14]. Among the investigated fibers, PVA/BA hybrid fibers exhibited the highest ultimate strength (41 % reduction), suggesting their effectiveness in stress distribution under increased shear span. Ductility improved significantly for all specimens by 32.5 %–108 % (except TPPL) after removing the haunches, indicating enhanced inelastic energy absorption. However, total energy absorption decreased by 16 %–68 % for all specimens due to reduced stiffness and ultimate strength. TPPL fibers outperformed PPL fibers in both ultimate strength (14.7 % higher) and cracking strength (25.7 % higher), potentially due to better stress transfer under shear. The post-peak energy dissipation difference between TPPL and PPL fibers became less significant after removing the haunches.

Removing haunches led to a significant decrease in ultimate strength and cracking strength for hybrid PPL/PVA (42.6 % and 47.3 % respectively), while the reduction for mono PPL was much smaller (7.7 % and 18.6 % higher than mono PPL). Total energy dissipation also decreased, with a 56 % drop for PPL and a 16 % reduction for hybrid PPL/PVA. Improved bonding between PPL and PVA fibers in the hybrid system helped distribute shear stresses, improve cracking strength, and absorb more energy, leading to superior ductility (3.31) compared to other fibers. This was attributed to improved micro-crack bridging by PVA fibers, enhancing inelastic behaviour. Removing haunches eliminated post-peak energy absorption for hybrid PVA/BA and significantly reduced total energy dissipation by 38 %.

#### 4.5. Group V: effect of SWSSC strength

The data presented in Table 6 demonstrates that a 60 % increase in concrete strength resulted in an elevation in the values of  $T_{GF}$ ,  $T_{FRC}$ , and  $C_c$ , while simultaneously decreasing the depth of the neutral axis ( $d_n$ ) compared to specimens with lower concrete strength. The introduction of compression reinforcement further contributed to an increase in  $d_n$  and a reduction in the tension zone of the cross-section. This effect contributed to a more efficient utilization of the compressive strength of concrete and enhanced the overall shear behaviour of the culverts.

High-strength concrete significantly enhanced the ultimate strength and cracking strength ( $P_{cr}$ ) of the C135-G1-PL.H specimen by 76.3 % and 78.8 %, respectively. For the C135-G2-PL.H specimen, the corresponding increases were 48 % and 9 %. This suggests that the impact of high-strength concrete on ultimate strength is more pronounced when only bottom reinforcement is employed. High-strength concrete also substantially improved the shear capacity of small culverts, leading to a notable increase in their ultimate bearing strength. This improvement was attributed to the increased compressive force exerted by the concrete within the compression zone of the crown section. The disparity in ultimate strength between C135-G1-PL.H and C135-G2-PL.H specimens was approximately 20 % for high-strength concrete, compared to 26 % for lower concrete strength, suggesting that top reinforcement was more effective with lower concrete strength. Compared to lower concrete strength, higher concrete strength allows the material to absorb a greater portion of the compressive load, reducing the reliance on top reinforcement. In contrast, for lower concrete strength, the addition of top reinforcement has a more significant impact on stress distribution and load-carrying capacity.

The C135-G1-PL.H specimen showed a significant 18 % increase in cracking strength when high-strength concrete was employed, but a 16 % decrease when lower-strength concrete was utilized. This difference was attributed to the improved bonding strength of PPL fibers with increasing concrete strength, facilitating enhanced tensile strength. Additionally, increasing concrete strength enhanced the total energy absorption ( $E_{tot}$ ) of the C135-G1-PL.H specimen by about 33 % but had no impact on the  $E_{tot}$  of the C135-G2-PL.H specimen. Interestingly, the pre-peak phase accounted for 71.6 % of the  $E_{tot}$  for the C135-G1-PL.H specimen compared to 87.9 % for the C135-G2-PL.H specimen. This suggests that increasing concrete strength and incorporating top reinforcement reduced the contribution of post-peak and inelastic behaviour, leading to a decrease in the ductility index ( $\mu_e$ ) of both specimens.

The contribution of the pre-peak stage to energy absorption increased significantly, from 63.4 % to 71.6 %, for the C135-G1-PL.H specimen due to the higher shear strength resulting from the use of high-strength concrete. The post-peak absorbed energy of the C135-G2-PL.H specimen improved by 66 % compared to the C135-G2-PL specimen, attributed to the enhanced bonding strength of PPL fibers in high-strength concrete, which facilitated crack bridging and energy dissipation. The difference in total energy absorption ( $E_{tot}$ ) between the C135-G1-PL.H and C135-G2-PL.H specimens was 33.8 %, while it was only 4.4 % for the C135-G1-PL and C135-G2-PL specimens. This highlights the effectiveness of increasing concrete strength in improving energy absorption, particularly when compression reinforcement is present. Additionally, the combined effect of PPL fiber incorporation and increased concrete strength resulted in a 73 % improvement in energy absorption compared to plain concrete culverts. However, the same combination led to only a 29 % increase when the top reinforcement was utilized. This could be attributed to the improved bonding strength between PPL fibers and the concrete matrix when higher concrete strength was used. Additionally, adding top reinforcement caused stress redistribution within the section and increased axial stiffness, which reduced deflection. These factors collectively contributed to a decrease in the effectiveness of PPL fibers on energy absorption.

### 5. Shear capacity prediction models

Extensive research highlights ongoing debate regarding the shear capacity of concrete culverts. This has led to numerous studies on the shear behaviour of steel-reinforced counterparts, with findings indicating higher observed shear strengths than predicted by design codes [42,55–58]. This section evaluates the shear capacity of GFRP-reinforced FR-SWSSC culverts using various standardized methods and presents a proposed shear capacity prediction. Five distinct approaches will be compared as described later. As the equations rely on

steel reinforcement, an equivalent steel ratio ( $\rho = \frac{E_{GFRP}}{E_s} \frac{A_{GFRP}}{bd}$ ) is employed to account for the GFRP bars.

### 5.1. Method-1: ACI 440.1R-15/RILEM TC-162

This method estimates the shear strength ( $V_n$ ) of fiber-reinforced concrete without stirrups by summing the individual contributions from the concrete ( $V_c$ ) and the fibers ( $V_f$ ). This approach has been previously applied to concrete beams reinforced with both GFRP bars and synthetic fibers [32]. According to ACI 440.1R-15, the shear capacity of concrete with internal FRP reinforcement is calculated using Eq. (4) and Eq. (5):

$$V_c = \frac{2}{5} \sqrt{f'_c} b_w k d \quad (4)$$

$$k = \sqrt{2\rho_f n_f + (\rho_f n_f)^2} - \rho_f n_f \quad (5)$$

Furthermore, the shear resistance of fibers ( $V_{fc}$ ) is determined according to Eq. (6), recommended by RILEM TC-162 [59].

$$V_{fc} = 0.7 k_f k_1 \tau_{fd} b d \quad (6)$$

The  $k_f$  and  $k_1$  factors account for the contributions of the flanges in a T-section and the size effect, respectively. These factors can be calculated as follows:

$$k_1 = 1 + \sqrt{\frac{200}{d}} \leq 2 \quad (7)$$

$$k_f = 1 + n \left( \frac{h_f}{b_w} \right) \left( \frac{h_f}{d} \right) \leq 1.5 \quad (8)$$

$$n = \frac{b_f - b_w}{h_f} \leq 3 \quad (9)$$

$$\tau_{fd} = 0.12 f_{R,4} \quad (10)$$

where  $d$  is effective depth of the top slab (mm),  $b_f$  is width of the flanges (mm),  $h_f$  is height of the flanges (mm),  $b_w$  is width of the web (mm),  $\tau_{fd}$  is shear strength due to fibers (MPa), and  $f_{R,4}$  is residual flexural strength of fiber-reinforced concrete (FRC) at CMOD = 3.5 mm (MPa).

### 5.2. Method-2: AS 5100.5

This method utilizes simplified equations from AS 5100.5 [60], where the ultimate shear capacity ( $V_u$ ) is attributed to both a concrete component ( $V_{uc}$ ) and an additional fiber-resisting component ( $V_{uf}$ ). Consequently,  $V_u$  can be calculated using the following equations:

$$V_u = V_{uc} + V_{uf} \quad (11)$$

$$V_{uc} = k_v \sqrt{f'_c} b d_v \quad (12)$$

$$k_v = \frac{200}{1000 + 1.3 d_v} \leq 0.1 \quad (13)$$

$$V_{uf} = 0.7 k_{\theta} f'_{1.5} b d_v \quad (14)$$

$$k_{\theta} = \cot \theta_v \leq 1.28 \quad (15)$$

$$f'_{1.5} = 0.4 f'_{R,4} - 0.07 f'_{R,2} \quad (16)$$

The variables  $f'_{R,4}$  and  $f'_{R,2}$  denote the average residual flexural strengths corresponding to crack CMOD of 3.5 mm and 1.5 mm, respectively. The term  $f'_{1.5}$  denotes the characteristic residual tensile strength of steel fiber-reinforced concrete (SFRC). The  $\theta_v$  represents the angle created

between the axis of the concrete compression strut and the longitudinal axis of member. The variable  $k_v$  represents the coefficient that measures the extent to which concrete contributes to shear strength, whereas  $d_v$  indicates the effective shear depth.

### 5.3. Method-3: AS 1597.2-2013

The Australian standard for steel-reinforced concrete culverts presents an alternative shear strength equation for culverts, derived from the following calculations applied to the critical shear section, where  $\frac{M_u}{\phi V_u d} = 3.0$ .

$$V_{uc} = v_b b d S_m \frac{F_D}{F_N} \quad (N) \quad (17)$$

$$v_b = 4.98(0.018334 + \rho) \sqrt{f'_c} \leq 0.191 \sqrt{f'_c} \quad (MPa) \quad (18)$$

$$S_m = \frac{4}{\left( \frac{M_u}{\phi V_u d} + 1 \right)} \quad (19)$$

$$F_D = 0.8 + \frac{40}{d} \leq 1.25 \quad (20)$$

$$F_N = 0.5 - \left( \frac{N_u}{6V_u} \right) + \sqrt{0.25 + \left( \frac{N_u}{6V_u} \right)^2} \quad (21)$$

where  $v_b$  denotes the nominal basic shear strength for locations where  $\frac{M_u}{\phi V_u d} \geq 3.0$ .  $F_D$  represents the depth factor, and  $F_N$  is the axial thrust factor.

### 5.4. Method-4: AASHTO LRFD 2020

a) The shear strength ( $V_c$ ) in kN of slabs in steel-reinforced box culverts with a fill depth of 0.61 m (2.0 ft) or greater, subjected to one-way action, shall be evaluated according to the following AASHTO-recommended equations [52,61]:

$$V_c = \left( 1.7756 \times 10^{-4} \lambda \sqrt{f'_c} + 0.03173 \frac{A_s}{b d_e} \frac{V_u d_e}{M_u} \right) b d_e \quad (22)$$

where  $\lambda$  denotes the concrete density modification factor,  $A_s$  represents the area of reinforcement within the design width ( $\text{mm}^2$ ),  $b$  signifies the design width (mm),  $d_e$  stands for the effective depth (mm),  $V_u$  is the shear force due to factored loads (kN), and  $M_u$  represents the factored moment at the section (kN.mm). If normal-weight concrete is employed,  $\lambda$  should be assigned a value of 1.0.

b) For one-way action of steel-reinforced box culvert slabs under a fill depth less than 0.61 m (2.0 ft), AASHTO provides the following equation for concrete shear strength:

$$V_c = 8.3 \times 10^{-5} \beta \lambda \sqrt{f'_c} b_v d_v \quad (23)$$

$$\beta = \frac{4.8}{(1 + 750 \varepsilon_f)} \frac{51}{(39 + s_{xe})} \quad (24)$$

$$\varepsilon_f = \frac{\frac{|M_u|}{d_v} + 0.5 N_u + |V_u|}{E_f A_f} \leq 0.006 \quad (25)$$

$$s_{xe} = s_x \frac{1.38}{a_g + 0.63} \quad (26)$$

$$304.8 \text{ mm} \leq s_{xe} \leq 2032.0 \text{ mm}.$$

where  $b_v$  and  $d_v$  denote the effective web width and effective shear depth, respectively. The factor  $\beta$  represents the ability of diagonally cracked concrete to transmit tension and shear.  $\varepsilon_s$  signifies the net longitudinal tensile strain within the section at the centroid of the tension

reinforcement, and  $s_{xe}$  denotes the crack spacing parameter influenced by aggregate size, while  $s_x$  stands for the crack spacing parameter.

c) For sections without transverse reinforcement, in the case of two-way action, the nominal shear resistance,  $V_c$ , of the concrete in kN, shall be determined as follows [61]:

$$V_c = 8.2933 \times 10^{-4} k \sqrt{f_c} b_o d_v \quad (27)$$

where  $k$  denotes the ratio of depth of neutral axis to depth of flexural reinforcement. The perimeter of the critical section for shear ( $b_o$ ) is expressed in mm.

##### 5.5. Method-5: ACI 440.1R-15 punching shear strength

According to ACI 440.1R-15 [24], Eq. (28) can be employed to calculate the punching shear capacity of two-way slabs. Given that the primary failure mode observed in the studied small culverts was punching shear, the applicability of this method was also investigated.

$$V_c = \frac{4}{5} \sqrt{f_c} b_o k d \quad (28)$$

##### 5.6. Comparison of the shear capacity prediction models

Fig. 15 presents the ratio of experimental shear strength ( $V_{exp}$ ) to predicted values ( $V_{pre}$ ) obtained from various methodologies. The findings revealed that ACI 440.1R-15/RILEM TC-162 demonstrably underestimated the shear capacity of the GFRP-reinforced small SWSSC culvert without fibers (C135-G1), while AS 1597.2-2013 and AASHTO 4-c overestimated. Other methods exhibit a reasonable underestimation of the shear strength of C135-G1 specimen, where AASHTO 4-a, AASHTO 4-b and ACI 440.1R-15 punching shear methods resulted in more accurate estimations.

For FR-SWSSC culverts illustrated in Fig. 15, the investigated methods demonstrated varying degrees of accuracy in predicting shear strength. The AASHTO 4-a, 4-b, and ACI 440.1R-15 punching shear methods consistently underestimated the capacity for all fiber types. In contrast, AASHTO 4-c significantly overestimated shear strength in culverts containing fibers, whether mono or hybrid. This could stem from the concept underlying this method, which is based on the two-way action of the crown. In contrast, the inverted U-shaped culverts investigated in this study exhibited one-way action due to the lack of lateral restraints, which aligns with the AASHTO 4-a and 4-b methods. Most methods underestimated shear strength for culverts with lower crown

thickness (C80), with AS 1597.2-2013 and AASHTO 4-c providing the most accurate estimates. The removal of haunches yielded reasonable estimates, except for AS 5100.5 and ACI 440.1R-15/RILEM TC-162, which significantly underestimated, and AASHTO 4-c and AS 1597.2-2013, which significantly overestimated. For high-strength concrete, AS 5100.5 and AS 1597.2-2013 provided reliable predictions.

##### 5.7. Proposed shear capacity prediction model

Based on a comparative analysis of various shear prediction models, this study proposes a modified model for GFRP-reinforced small SWSSC culverts. This proposed model incorporates two primary components: the punching shear strength of the crown with GFRP reinforcement ( $V_c$ ) and that due to fiber-reinforced concrete ( $V_{uf}$ ). The analysis revealed that ACI 440.1R-15 underestimates the shear capacity of the culverts, primarily due to neglecting fiber effects. By incorporating the fiber-reinforced concrete shear strength from AS5100.5 and adjusting for fiber type and hybridization, this study presents the proposed model. Eq. (29) to Eq. (33) outline the calculation method, where  $k_h$  represents the haunch effect and  $f'_{R,1}$  denotes the residual flexural strength of FRC at CMOD = 0.5 mm in MPa.

$$V = V_c + V_{uf} \quad (29)$$

$$V_c = \frac{4}{5} \sqrt{f_c} b_o k d \quad (30)$$

$$V_{uf} = 0.7 k_h k_{f,1.5} b d_v \quad (31)$$

$$f_{1.5} = \begin{cases} 0.4 f'_{R,4} - 0.07 f'_{R,2}, & \text{others} \\ 0.3 f'_{R,1}, & BA/PV \end{cases} \quad (32)$$

$$k_h = \begin{cases} 1.0, & \text{with haunches} \\ 0.7, & \text{without haunches} \end{cases} \quad (33)$$

Previous investigations have shown that hybrid BA/PV fibers exhibit superior performance in fracture toughness tests at low deflection levels and immediately following the peak load [20]. This suggests that a CMOD of 0.5 mm would be optimal for hybrid BA/PV fibers in such applications. Furthermore, this study revealed that for specimens without haunches, the  $V_{uf}$  should be reduced by 30 % to account for the influence of haunches on the shear capacity of small concrete culverts.

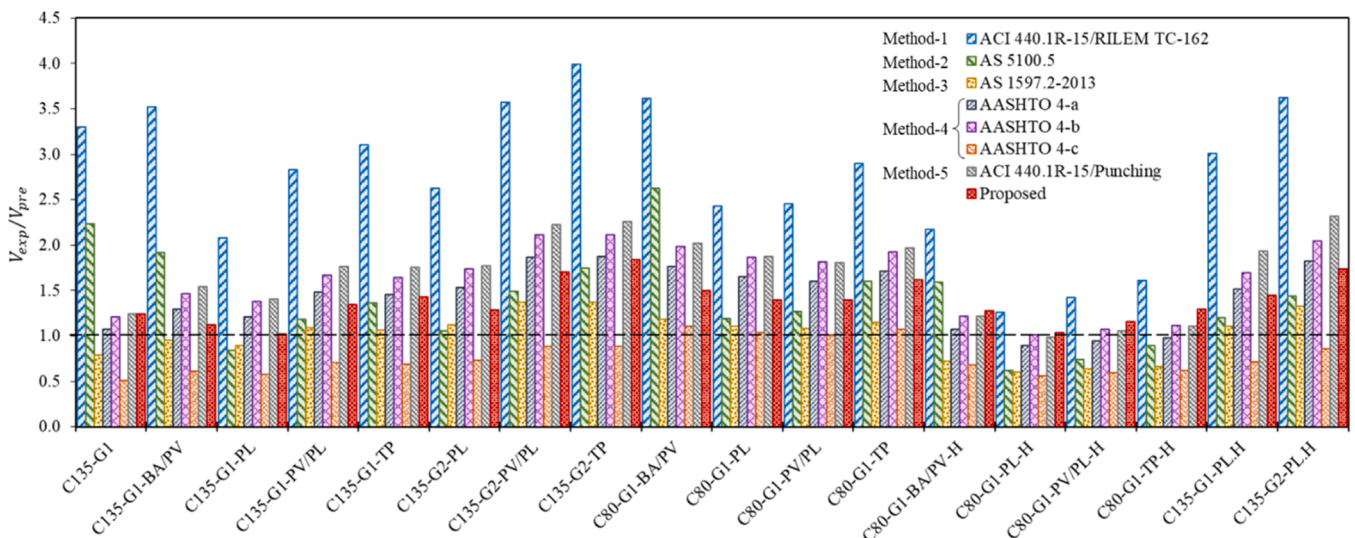


Fig. 15. Comparison of experimental and predicted shear capacity for GFRP reinforced concrete culverts.

## 6. Summary and conclusion

An experimental study examined the behaviour of small SWSSC culverts reinforced with GFRP bars and fibers. Eighteen FR-SWSSC culverts were tested according to AS 1597.2–2013. The study evaluated various parameters that affect culvert behaviour, including fiber type, compression GFRP reinforcement, crown thickness, haunches, and concrete strength. The experimental study yielded the following conclusions:

- Shear failure was the primary mode of failure in all culverts, characterized by a diagonal shear crack propagating from the load point to the haunch. This could be attributed to the limited shear capacity of GFRP bars in the transverse direction. Fiber incorporation potentially modified crack patterns and improved post-peak performance.
- TPPL fibers increased ultimate strength by 49.7 % and energy dissipation by 47 % over plain SWSSC culverts, outperforming PPL fibers by 31.8 % and 13 %, respectively. TPPL and PPL fibers enhanced cracking strength by 19.7 % and 15.5 %. The improved performance was likely due to the better distribution and mechanical bonding of TPPL fibers, enhancing elasticity, while PPL fibers favoured pull-out and inelastic behaviour.
- PPL/PVA hybridization improved shear stress distribution and increased ultimate strength by 47.1 % over SWSSC culverts and 29.5 % over PPL culverts. It also improved cracking strength by 18 % compared to mono PPL fibers, preserved total energy dissipation, and achieved 73 % higher pre-peak dissipation, but reduced ductility compared to the control specimen. This improvement was likely due to the higher tensile strength and strong chemical bond of PVA fibers with the concrete matrix, which, in synergy with PPL fibers, increased stiffness, reduced ductility, and enhanced pre-peak energy dissipation.
- Micro-fiber hybridization (PVA/BA) increased ultimate strength, first-cracking strength, and ductility by 29 %, 49.3 % and 34 %, respectively, compared to plain SWSSC culvert. Additionally, it improved energy absorption and ultimate strength by 14.6 % and 13.6 %, respectively, over PPL fibers. This improvement was attributed to the positive synergy of PVA/BA hybridization and the superior strength and stiffness of BA, which contributed to increased stiffness, effective distribution of shear stresses, and improved pre-peak behaviour of the culverts.
- The addition of top reinforcement increased ultimate strength (up to 28 %) and first-cracking strength (up to 22 %) but reduced ductility and energy dissipation. This could be attributed to the enhanced axial stiffness provided by the compression reinforcement. Hybridizing PPL/PVA fibers improved stiffness compared to PPL fibers alone, resulting in 15 % higher ductility and 28 % higher energy absorption, compared to specimens without top reinforcement, indicating enhanced performance in the presence of compression reinforcement.
- Reducing crown thickness by 40 % significantly decreased the strength, energy absorption, and ductility of fiber-reinforced culverts. Thicker crowns distributed stress better, enhancing fiber performance and ductility, while thinner crowns concentrated stress, reducing effectiveness. TPPL fibers improved cracking strength in thinner slabs, increasing total energy absorption by 55 %, with a sevenfold increase in post-peak absorption and 19.7 % higher ductility than PPL fibers.
- Removing haunches increased the shear span and reduced stiffness, reducing shear strength and energy absorption by 16 % to 68 % but improving ductility by 32.5 % to 108 % (excluding TPPL). TPPL fibers showed 14.7 % higher ultimate strength and 25.7 % higher cracking strength than PPL fibers, likely due to better stress distribution. PVA/BA hybrid fibers had the highest ultimate strength and

stress distribution, but energy dissipation decreased by 38 % and post-peak absorption was eliminated after removing haunches.

- A 60 % increase in concrete strength improved the ultimate and cracking strength of PPL-reinforced culverts by 76.3 % and 78.8 %, respectively, with only bottom reinforcement. This suggests that top reinforcement was more effective with lower concrete strength. Higher concrete strength enhanced PPL fiber bonding and compressive load absorption, reducing the need for top reinforcement. For lower concrete strength, top reinforcement significantly increased stress distribution and load-carrying capacity.
- The AASHTO equations for steel-reinforced concrete box culverts, based on one-way crown action, reliably predicted the shear capacity of small GFRP-reinforced concrete culverts with fiber inclusions, though with some underestimation. This can be attributed to the one-way action observed in the crown of the investigated culverts, resulting from the lack of lateral restraint. The proposed model, considering GFRP bars, punching shear failure, haunches, and crown thickness, offered more accurate predictions.

## CRediT authorship contribution statement

**Allan Manalo:** Writing – review & editing, Supervision. **Christopher Chow:** Writing – review & editing, Supervision. **Milad Bazli:** Writing – review & editing, Software. **Reza Hassanli:** Writing – review & editing, Supervision, Investigation, Conceptualization. **Amirhesam Mashayekhi:** Writing – original draft, Methodology, Data curation, Conceptualization. **Xing Ma:** Writing – review & editing, Supervision. **Yan Zhuge:** Writing – review & editing, Supervision.

## Acknowledgements

The authors gratefully acknowledge the financial support provided by the University of South Australia. We extend our appreciation to the university's concrete laboratory technicians for their technical expertise. We also thank Adelaide Brighton Cement Ltd and Independent Cement and Lime Pty Ltd for their generous donations of OPC and GGBS, respectively, and TEXO for supplying TPPL fibers, and the support of Mr. Adam Bromley. We would like to express our gratitude to Dr. Murray Townsend and Mr. Mojtaba Karbasi from the Department for Environment and Water (DEW), as well as Mr. Spiros Dimas from the Department for Infrastructure and Transport (DIT) in the Government of South Australia, for their invaluable support in providing sea sand. Additionally, we recognize the valuable instrumentation and expertise provided by Microscopy Australia at the Future Industries Institute, University of South Australia.

## Appendix A. Supporting information

Supplementary data associated with this article can be found in the online version at [doi:10.1016/j.istruc.2024.107492](https://doi.org/10.1016/j.istruc.2024.107492).

## References

- [1] Xiao L, Hu H, Peng S, Du Z, Xu C. Compression behavior of GFRP reinforced hybrid fibre reinforced concrete short columns subjected to eccentric loading. *Constr Build Mater* 2023;393:131985.
- [2] Mostafa IT, Mousa S, Mohamed HM, Benmokrane B. Experimental and analytical behavior of GFRP-reinforced concrete box girders under pure torsion. *J Compos Constr* 2024;28(1):04023064.
- [3] Manalo A, Mendis P, Bai Y, Jachmann B, Sorbello C. Fiber-reinforced polymer bars for concrete structures: state-of-the-practice in Australia. *J Compos Constr* 2021;25(1):05020007.
- [4] Zhang P, Shang J, Liu Y, Shao J, Gao D, Dong Z, Sheikh SA. Flexural behavior of GFRP bar-reinforced concrete beams with U-shaped UHPC stay-in-place formworks. *J Build Eng* 2022;45:103403.
- [5] Amran YM, Alyousef R, Rashid RS, Alabduljabbar H, Hung C-C. Properties and applications of FRP in strengthening RC structures: A review. *Structures*. Elsevier; 2018.



- [6] Alkhrdaji T, Nanni A. Design, construction, and field-testing of an RC Box Culvert Bridge reinforced with GFRP bars. *Non-Metallic Reinforcement for Concrete Structures-FRPRCS* 2001;5.
- [7] Hassanli R, Youssf O, Manalo A, Najafgholipour MA, Elchalakani M, del Rey Castillo E, Lutz D. An experimental study of the behavior of GFRP-reinforced precast concrete culverts. *J Compos Constr* 2022;26(5):04022043.
- [8] Gooranorimi O, Nanni A. GFRP reinforcement in concrete after 15 years of service. *J Compos Constr* 2017;21(5):04017024.
- [9] Wang Z, Zhao X-L, Xian G, Wu G, Raman RS, Al-Saadi S, Haque A. Long-term durability of basalt-and glass-fibre reinforced polymer (BFRP/GFRP) bars in seawater and sea sand concrete environment. *Constr Build Mater* 2017;139: 467–89.
- [10] D'Antino T, Pisani M, Poggi C. Effect of the environment on the performance of GFRP reinforcing bars. *Compos Part B: Eng* 2018;141:123–36.
- [11] Wang Z, Zhao X-L, Xian G, Wu G, Raman RS, Al-Saadi S. Effect of sustained load and seawater and sea sand concrete environment on durability of basalt-and glass-fibre reinforced polymer (B/GFRP) bars. *Corros Sci* 2018;138:200–18.
- [12] Tjaronge MW, Irfan UR. Porosity, pore size and compressive strength of self compacting concrete using sea water. *Procedia Eng* 2015;125:832–7.
- [13] Vafaei D, Ma X, Hassanli R, Duan J, Zhuge Y. Experimental study on cyclic flexural behaviour of GFRP-reinforced seawater sea-sand concrete slabs with synthetic fibres. *Ocean Eng* 2023;273:114014.
- [14] Zhou L, Zheng Y, Di B, Lv J, Taylor SE. Shear behaviour of SWSS-SCC beams reinforced with GFRP bars and stirrups: Experimental and analytical investigations. in *Structures*. Elsevier; 2023.
- [15] Wang Z, Xie J, Li J, Liu P, Shi C, Lu Z. Flexural behaviour of seawater-sea sand concrete beams reinforced with GFRP bars: effects of the reinforcement ratio, stirrup ratio, shear span ratio and prestress level. *J Build Eng* 2022;54:104566.
- [16] Chen Z, Li S, Zhou J, Xu R, Dai S. Flexural behavior of GFRP bars reinforced seawater sea sand concrete beams exposed to marine environment: experimental and numerical study. *Constr Build Mater* 2022;349:128784.
- [17] Mashayekhi A, Hassanli R, Zhuge Y, Ma X, Chow CW. Synergistic effects of fiber hybridization on the mechanical performance of seawater sea-sand concrete. *Constr Build Mater* 2024;416:135087.
- [18] Huang Y, He X, Wang Q, Sun Y. Mechanical properties of sea sand recycled aggregate concrete under axial compression. *Constr Build Mater* 2018;175:55–63.
- [19] Huang Y, Wang T, Sun H, Li C, Yin L, Wang Q. Mechanical properties of fibre reinforced seawater sea-sand recycled aggregate concrete under axial compression. *Constr Build Mater* 2022;331:127338.
- [20] Mashayekhi A, Hassanli R, Zhuge Y, Ma X, Chow CW, Bazli M, Manalo A. Synergistic effects of fiber hybridization on the fracture toughness of seawater sea-sand concrete. *Constr Build Mater* 2024;444:137845.
- [21] Zeng J-J, Liao J, Zhuge Y, Guo Y-C, Zhou J-K, Huang Z-H, Zhang L. Bond behavior between GFRP bars and seawater sea-sand fiber-reinforced ultra-high strength concrete. *Eng Struct* 2022;254:113787.
- [22] Xiong Z, Zeng Y, Li L, Kwan A, He S. Experimental study on the effects of glass fibres and expansive agent on the bond behaviour of glass/basalt FRP bars in seawater sea-sand concrete. *Constr Build Mater* 2021;274:122100.
- [23] Mahaini Z, Abed F, Alhoubi Y, Elnessar Z. Experimental and numerical study of the flexural response of Ultra High Performance Concrete (UHPC) beams reinforced with GFRP. *Compos Struct* 2023;315:117017.
- [24] Institute AC. Guide for the Design and Construction of Structural Concrete Reinforced with FRP Bars (ACI-440.1R-15). American Concrete Institute; 2015.
- [25] Vafaei D, Hassanli R, Ma X, Duan J, Zhuge Y. Sorptivity and mechanical properties of fiber-reinforced concrete made with seawater and dredged sea-sand. *Constr Build Mater* 2021;270:121436.
- [26] Vafaei D, Hassanli R, Ma X, Duan J, Zhuge Y. Fracture toughness and impact resistance of fiber-reinforced seawater sea-sand concrete. *J Mater Civ Eng* 2022;34(5):04022038.
- [27] Chenggong Z, Zhiyuan W, Zhenyu Z, Qiuyu G, Xinrui W, Renda Z. Research on different types of fiber reinforced concrete in recent years: An overview. *Constr Build Mater* 2023;365:130075.
- [28] Kaidi J, Xin W, Lining D, Zhiyuan C, Huang H, Xia L, Jianxun L, Zhishen W. Mechanical properties of multi-scale mono/hybrid non-metallic fiber-reinforced ultra-high performance seawater sea-sand concrete. *Constr Build Mater* 2023;401: 132922.
- [29] Huang H, Yuan Y, Zhang W, Hao R, Zeng J. Bond properties between GFRP bars and hybrid fiber-reinforced concrete containing three types of artificial fibers. *Constr Build Mater* 2020;250:118857.
- [30] Xiao L, Dai S, Jin Q, Peng S. Bond performance of GFRP bars embedded in steel-PVA hybrid fiber concrete subjected to repeated loading. *Struct Concr* 2023;24(1): 1597–611.
- [31] Vakili SE, Homami P, Esfahani MR. Effect of fibers and hybrid fibers on the shear strength of lightweight concrete beams reinforced with GFRP bars. *Structures*. Elsevier; 2019.
- [32] Dev A, Chellapandian M, Prakash SS. Effect of macrosynthetic and hybrid fibers on shear behavior of concrete beams reinforced with GFRP bars. *J Bridge Eng* 2020;25(7):04020031.
- [33] Patil GM, Chellapandian M, Prakash SS. Effectiveness of hybrid fibers on flexural behavior of concrete beams reinforced with glass fiber-reinforced polymer bars. *Acids Struct J* 2020;117(5).
- [34] Ramesh B, Eswari S, Sundararajan T. Flexural behaviour of glass fibre reinforced polymer (GFRP) laminated hybrid-fibre reinforced concrete beams. *SN Appl Sci* 2020;2:1–10.
- [35] Standard, A., Specification and supply of concrete, AS 1379–2007, Australia. 2007.
- [36] AS1597.2, Precast reinforced concrete box culverts, Part 2: Large culverts (exceeding 1200 mm span or 1200 mm height and up to and including 4200 mm span and 4200 mm height). 2013, Standards Australia.
- [37] Mashayekhi A, Hassanli R, Zhuge Y, Ma X, Chow CW. Cyclic flexural performance of seawater sea-sand concrete reinforced with hybrid fibers. *Constr Build Mater* 2024;449:138480.
- [38] Pakravan HR, Ozbakkaloglu T. Synthetic fibers for cementitious composites: a critical and in-depth review of recent advances. *Constr Build Mater* 2019;207: 491–518.
- [39] AS1597.1, Precast reinforced concrete box culverts, Part 1: Small culverts (not exceeding 1200 mm span and 1200 mm height). 2010, Standards Australia.
- [40] Ramadan SH, Naggar MHEL. Design guidelines for reinforced concrete three-sided culverts. *Tunn Undergr Space Technol* 2022;119:104259.
- [41] Ramadan SH, El Naggar MH. Effect of large-span three-sided culvert configuration on its performance at service and ultimate loading conditions. *Tunn Undergr Space Technol* 2022;122:104346.
- [42] Abolmaali A, Garg AK. Effect of wheel live load on shear behavior of precast reinforced concrete box culverts. *J Bridge Eng* 2008;13(1):93–9.
- [43] AlHamaydeh M, Orabi Manwar. Punching shear behavior of synthetic fiber-reinforced self-consolidating concrete flat slabs with GFRP bars. *J Compos Constr* 2021;25(4):04021029.
- [44] Hassanli R, Manalo A, Vafaei D, Yekrangnia M, Elchalakani M, Noël M. Cyclic behavior of GFRP-reinforced concrete one-way slabs with synthetic fibers. *J Build Eng* 2023;65:105741.
- [45] Hassanli R, Youssf O, El-Naqeeb MH, Yekrangnia M, Elchalakani M, Ghanbari-Ghazijahani T, Bazli M. Investigation of punching shear performance in concrete slabs reinforced with GFRP and synthetic fibers: an experimental study. *Eng Struct* 2024;311:118215.
- [46] Guo Z. Principles of reinforced concrete. Butterworth-Heinemann; 2014.
- [47] Abdel-Karim AH, Khalil GI, Eweis AE, Makhlof MH. Impact of developed hybrid polypropylene fiber inclusion on the flexural performance of concrete beams reinforced with innovative hybrid bars. *Constr Build Mater* 2023;409:134113.
- [48] Akin SK, Kartal S, Müsevitoglu A, Sancioğlu S, Zia AJ, İlgin A. Macro and micro polypropylene fiber effect on reinforced concrete beams with insufficient lap splice length. *Case Stud Constr Mater* 2022;16:e01005.
- [49] Guide for the Design and Construction of Structural Concrete Reinforced with Fiber-Reinforced Polymer FRP Bars. American Concrete Institute; 2015. ACI-440.1R-15.
- [50] ACI A. 544.4 R-88 Design considerations for steel fibre reinforced concrete. *Am Concr Inst Aids Said Comm* 1988;544.
- [51] Shanour AS, Said M, Arafa AI, Maher A. Flexural performance of concrete beams containing engineered cementitious composites. *Constr Build Mater* 2018;180: 23–34.
- [52] AASHTO, LRFD Bridge Design Specifications. 2020, American Association of State Highway and Transportation Officials, Washington, DC.
- [53] Mostafazadeh M, Abolmaali A, Ghahremannejad M. Shear strength of synthetic fiber-reinforced concrete box culverts. *J Bridge Eng* 2019;24(6):04019039.
- [54] Naaman A, Jeong M. 45 Structural ductility of concrete beams prestressed with FRP tendons. *Non-Metallic (FRP) Reinforcement for concrete structures: proceedings of the second international RILEM symposium*. CRC Press; 1995.
- [55] Garg AK, Abolmaali A, Fernandez R. Experimental investigation of shear capacity of precast reinforced concrete box culverts. *J Bridge Eng* 2007;12(4):511–7.
- [56] Garg AK, Abolmaali A. Finite-element modeling and analysis of reinforced concrete box culverts. *J Transp Eng* 2009;135(3):121–8.
- [57] Yee, R.A., Shear behaviour of concrete box culverts. 2004.
- [58] Ghahremannejad M, Abolmaali A, Mahdavi M. Shear strength of top slab of reinforced concrete box culverts. *Acids Struct J* 2019;116(6):63–74.
- [59] TC162-TDF R. Test and design methods for steel fibre reinforced concrete. *Mater Struct* 2003;36:560–7.
- [60] Standard A. Bridge design–part 5: Concrete; 2017. p. AS5100.5.
- [61] Highway, A.Ao.S. and T. Officials, AASHTO LRFD Bridge Design Guide Specifications for GFRP-Reinforced Concrete. 2018: American Association of State Highway and Transportation Officials.